PERIODICO di MINERALOGIA
established in 1930

Dipartimento di Scienze della Terra
Sapienza Università di Roma

An International Journal of
Mineralogy, Crystallography, Geochemistry,
Ore Deposits, Petrology, Volcanology
and applied topics on Environment, Archaeometry and Cultural Heritage

U-Pb zircon ages, geochemistry and tectonic setting of felsic and mafic intrusive rocks of Almogholagh complex, NW Iran

Mahboobeh Jamshidibadr [1,*], Alan S. Collins [2], Gabriel N. Salomao [2], Mozaniel Costa [2]

[1] Geology Department, Payam Noor University, 19395-4697 Tehran, I.R of Iran
[2] Tectonics, Resources and Exploration (TRaX), School of Earth and Environmental Sciences, University of Adelaide, SA 5005, Australia

ARTICLE INFO

Submitted: November 2017
Accepted: March 2018
Available on line: April 2018

* Corresponding author:
m_jamshidi@pnu.ac.ir

DOI: 10.2451/2018PM761

How to cite this article:
Jamshidibadr M. et al. (2018)
Period. Mineral. 87, 21-53

ABSTRACT

The Almogholagh Complex is a part of Sanandaj-Sirjan Zone that outcrops in the northwest of this zone and contain felsic and mafic rocks. LA-ICP-MS zircon U-Pb age of felsic rocks between 148 to 143 Ma. The felsic rock, which shows a high-K calc-alkaline affinity, enrichment in LREEs compared to the HREEs and the high values of Yb and Y, low Sr, and negative Eu anomaly imply that source is within the stability field of plagioclase. High SiO2 and low MgO contents in felsic rocks suggest that the mantle cannot directly produce this magma while the intergrowth texture of K-feldspar and quartz implies crystallization around the K-feldspar-quartz eutectic at lower temperatures. It can be concluded that the high-K felsic rocks did not originate directly from the mantle source, as do most I-type, calc-alkaline granitoids, but more likely originated from the partial melting of pre-existing I-type granitoids in the upper continental crust under low-pressure conditions.

Considering the low Yb and Y concentrations, a high Sr, a very weak anomaly in Eu, and a slight enrichment in LREEs compared to the HREEs in mafic rocks, it can be concluded that the origin of the magma is related to the stability field of garnet. Geochemical characteristics of mafic rocks show that their origin is associated with island arc of subduction area. Although the geochemical and magma relationships between the felsic and mafic rocks cannot be documented, emplacements of these intrusive rocks show distinct different trends in Neotethys subduction basin.

Keywords: U-Pb zircon geochronology; Almogholagh complex; Sanandaj-Sirjan zone.

INTRODUCTION

The convergence of Alpine-Himalayan belt as one the main continental orogenic belt represents typical continental collision including suture zones and micro-continental blocks. This belt, which extends from the eastern Mediterranean region to the Himalayas, has been originated as a result of the Neotethys Ocean closure (Ricou, 1994; Stampfli and Borel, 2002; Rolland et al., 2009; Trifonov et al., 2012; Tian et al., 2015) (Figure 1a).

The Zagros orogeny is the main central area of the Alpine-Himalayan orogenic belt formed as a result of the long-lasting convergence between the Iranian edge of Eurasia and Arabian plate as a part of Gondwana (Agard et al., 2011). The closure of the Neotethys oceanic entry over the Arabia-Eurasia collision caused separation of the Mediterranean Sea and Indian Ocean (Allen and Armstrong, 2008; Okay et al., 2010) (Figure 1a).

The Sanandaj-Sirjan Zone (SSZ) is the magmatic and

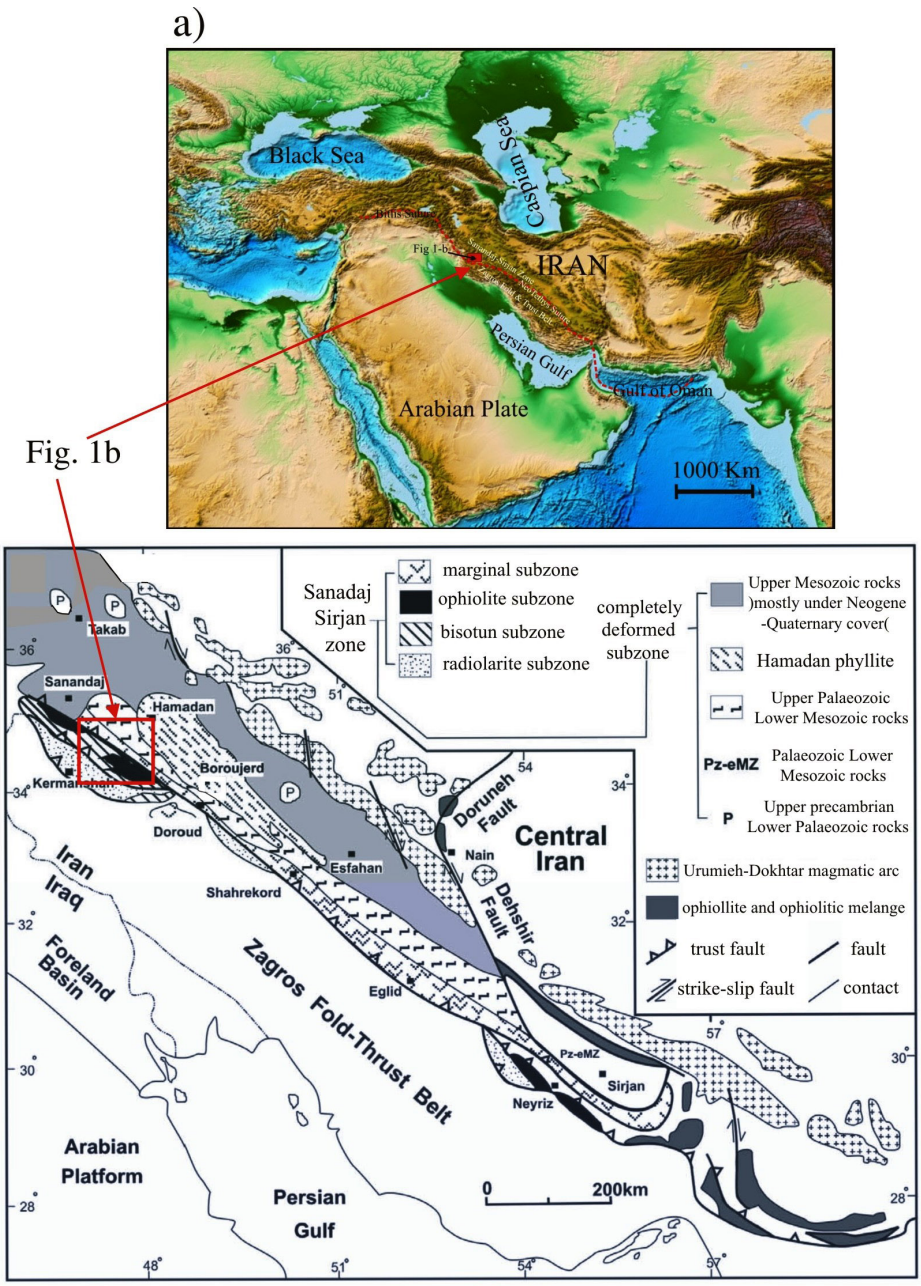

Figure 1a. Location of Sanandaj-Sirjan Zone. The Sanandaj-Sirjan Zone occurs between the Urumieh-Dokhtar Magmatic Arc and the Zagros Fold-Thrust Belt (after Mohajjel et al., 2003).

metamorphic region of the Zagros orogeny (Agard et al., 2005), overlays the Precambrian to Paleozoic sequences and contains calc-alkaline volcanic rocks and I-type granitoids originated throughout Late Jurassic to Upper Cretaceous periods. The petrogenesis of the granitoids and related volcanic rocks has been extensively associated with Neotethys subduction under the Iranian plate. It is proposed that after Late Triassic times the SSZ has become an active margin related with the accumulation prism (Sheikholeslami et al., 2008; Hassanzadeh and Wernicke, 2016). SSZ consists of sedimentary Paleozoic to Cretaceous and both HP/LT and HT/LP metamorphic rocks originated in an accretionary prism in the southern area of the Iranian microcontinent (Mouthereau, 2011; Jamshidi badr et al., 2010; Jamshidi badr et al., 2012).

The formation of SSZ with the 1500 km length and 150-200 km width is related to the Permian opening of the Neotethys Ocean (Muttoni et al., 2003) and its consequent

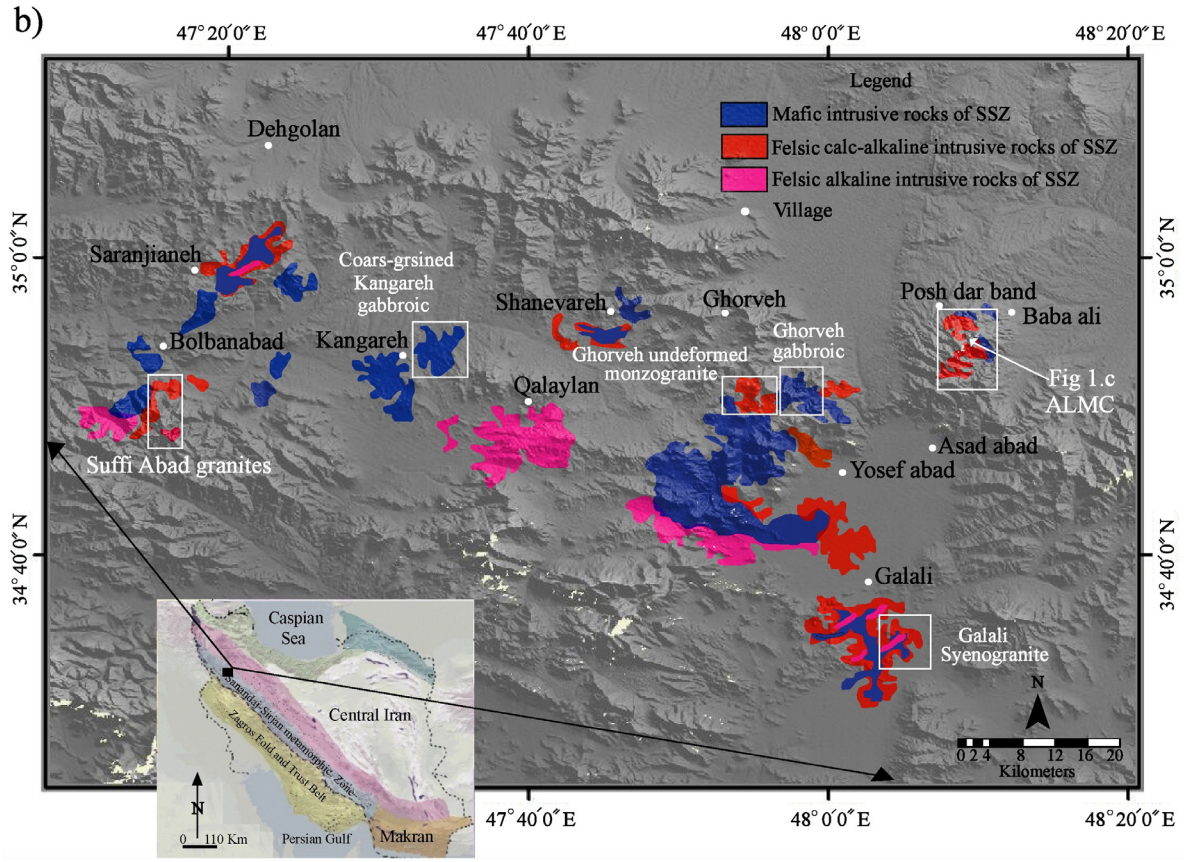

Figure 1b. Outcrops of felsic and mafic intrusives in the north of Sanandaj-Sirjan Zone (SSZ). The ALMC square shows the study rock.

subduction over convergence of Mesozoic to Cenozoic and continental collision at convergent boundaries of two plates of the Afro-Arabian and the Eurasian (Trifonov et al., 2012; Mohajjel et al., 2003; Ghasemi and Talbot, 2006; Moritz et al., 2006). The timing of continental drift of the Central Iran and Arabian plates has been attributed to Permian to Late Triassic (Hassanzadeh and Wernicke, 2016; Ghasemi and Talbot, 2006) Late Triassic to Early Jurassic (e.g. Stampfli and Borel, 2002; Agard et al., 2005; Davoudzadeh and Schmidt, 1984), or Middle Jurassic (Fazlnia et al., 2009). According to Okay and Tüysüz (1999), the Neotethys caused a distinct ocean over the Early Triassic periods. Consequently, most of the studies in the literature report that Neotethys Ocean has been originated during the Late Triassic or Early Jurassic (Stampfli and Borel, 2002) According to a new formation mechanism proposed for SSZ by Hassanzadeh and Wernicke (2016), the SSZ records the Permian breakup of Gondwana land, the Permian-Triassic drift history of the Cimmerian continent, latest Triassic/Early Jurassic subduction initiation, and the Jurassic through Paleogene propagation of arc magmatism beside the southern margin of Eurasia.

Hassanzadeh and Wernicke (2016) have collected the basic age and compositional data on >60 plutonic centers with an age range of the late Proterozoic to the late Miocene. Age distribution histograms presents five principal plutonic episodes at (1) late Proterozoic-Cambrian, (2) late Carboniferous-Early Permian, (3) early and middle Jurassic (volumetrically the most important event, with a conspicuous maximum at ~170 Ma), (4) Cretaceous-Paleogene in the northwestern SSA (which appears to continuation be of the Jurassic event), and (5) Miocene subvolcanic porphyries of the Qorveh-Takab region.

Jurassic igneous intrusions of SSZ have calc-alkaline affinity and arc-related geochemical signatures (Arvin et al., 2007; Ahmadi-Khalaji et al., 2007; Fazlnia et al., 2009; Fazlnia et al., 2013; Shahbazi et al., 2010; Ahadnejad et al., 2011; Mahmoudi et al., 2011; Esna-Ashari et al., 2012; Jamshidi badr et al., 2013; Hunziker et al., 2015). While most of the granitoids are I-type, some A-type examples have been also recognized through the region (e.g, Sarjoughian et al., 2015; Yajam et al., 2015). Note that the classification of granites, such as I-, S-, and A-types,

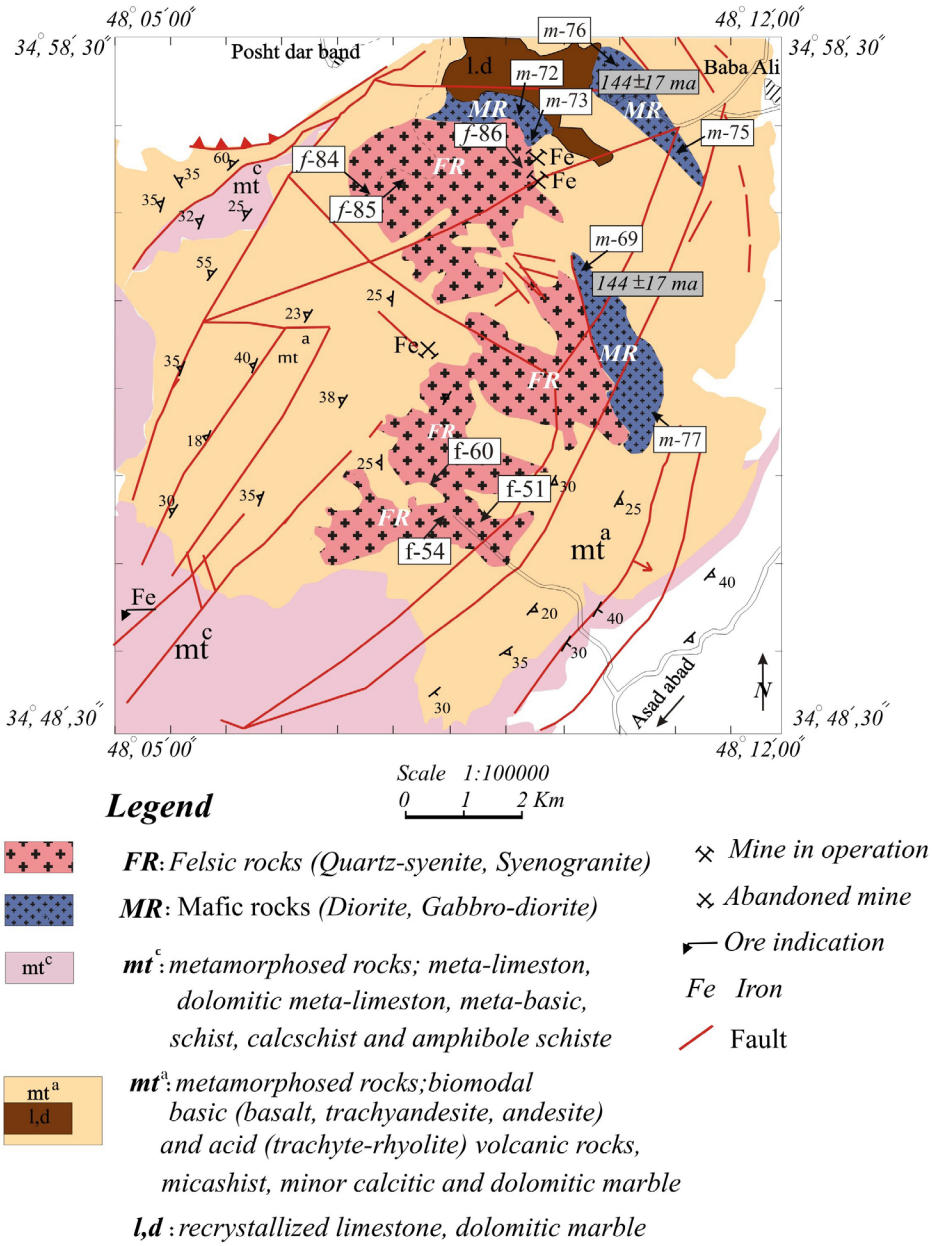

Figure 1c. Simplified geological map of the Almogholagh Complex (ALMC) after the Tuyserkan 1/100000 geological map (Ashragi and Mahmoudi Garaii, 2003); the location of analyzed samples is shown.

refer to their different magma sources (e.g. Chappell and White, 1974; Loiselle and Wones, 1979; Collins et al., 1982; Chappell et al., 1987, 1998; Whalen et al., 1987; Sylvester, 1989; Bonin, 2007). However, several granitic rocks cannot be related to classic granite classifications, like I-, A-, and S-types, due to their chemical and isotopic components belonging to two classes; for example, the Conway granite belongs to both groups of White Mountains, New Hampshire (Eby et al., 1992). In these cases, it is complex to form the tectonic setting in which the granite has been originated. For example, the direction of Hercynian and Caledonian granites is mostly from the mantle with some influence from the continental crust. However, several juvenile granites are poorly influenced by continental crust and directed in active margins or island arcs. According to Jahn et al. (2000), in China and Mongolia with the maximum number of juvenile granites, the juvenile granites show large value for the isotope ratio of $^{143}Nd/^{144}Nd$ and small value for $^{87}Sr/^{86}Sr$ isotope ratio. These ratios are as same as the basic rocks of oceanic

islands or subduction magmatic arcs, and juvenile granites occasionally display a near attraction toward A-type granites (Eby, 1990; Azizi and Asahara, 2013).

Intrusive rocks of Almogholagh complex (ALMC) are a part of SSZ. The intrusive rocks of ALMC are intrusions of SSZ located in the northwest Iran (Figure 1). The SSZ is located in the west area of the Iranian Plateau and is isolated from the plate of Arabian through the suture of Zagros. The characterization of this zone is performed using a dismembered upper Cretaceous to Palaeocene ophiolite manufactured from bodies of Eocene to Oligo-Miocene gabbroic, signifying that ultimate collision between Arabia and Eurasia happened in the mid-Tertiary period (Agard et al., 2005; Hassanzadeh and Wernicke, 2016; Azizi and Moinevaziri, 2009).

The purpose of the current research is to determine the age and geochemical features of intrusive rocks in SSZ for completing the outcomes of the earlier studies.

In the present study, the age of felsic rocks of ALMC was determined by new U-Pb zircon dating and geochemical features of felsic and mafic intrusive rocks of AlMC was discussed to determine the tectonic setting of these rocks and their relationship with other SSZ intrusive rocks.

General Geology of Almogholagh Complex (AlMC)

The ALMC is in 15 km northwest of the city of Hamedan in the northwestern Iran within 48°05′00″ to 48°12′00″ E longitude and 34°48′30″ to 34°58′30″ N latitude (Figure 1 a,b,c). The ALMC was first described on the 1:100000 geological map of Tuyserkan (Ashragi and Mahmoudi Garaii, 2003). The study area consists of several metasedimentary units, which are metamorphosed to greenschist facies and includes an intrusive complex with felsic and mafic composition. The oldest meta-sedimentary rocks are exposed around Almogholagh Mountain and contains dolomitic to calcitic marble and felsic metavolcanic rocks. Two suites of plutonic rock can be distinguished by their lithological features and the intrusive rock in the ALMC as:

- Gray to dark gray mafic intrusive rocks outcrop at three localities (Figure 1 b,c). Its extension is much more restricted than mafic intrusive elsewhere in the SSZ (Figure 1b). It has a granular and intergranular texture and contains plagioclase, clinopyroxene, and amphibole. Rb-Sr whole-rock dating yielded an age of 144±17 Ma (Late Jurassic to Early Cretaceous periods) (Valizadeh and Zarian, 1976).

- Light gray felsic intrusive rocks outcrop in the central part of the ALMC (Figure 1 b,c).

- Jamshidibadr (2013) defined four deformation steps for the ALMC. These steps are three ductile stages, which are followed by a brittle deformation phase. The first phase is the formation of the first group of folds and foliation. The second one is the formation of the second group of folds on a horizontal-to-sub-horizontal axial plane and a general NW-SE direction (parallel to the general trend of the SSZ). The third phase involves three groups of folds with vertical axial surfaces and horizontal axes originated through flexural-sliding. The outcropping associated with this phase are observed in 3 km northwest of the village of Chenar close to an iron mine. The brittle deformation step with noticeable faulting is seen in 5 km west of the village of Baba Ali near the summit of Almogholagh Mountain.

EXPERIMENTAL

Microprobe microanalysis

Minerals were selected for analysis using a Cameca SX100 electron microprobe at the Iran Mineral Processing Research Center. Quantitative analysis of selected minerals was performed with a 15 keV accelerating voltage using a 20 nA beam current and a 2-5 μm beam diameter. The counting time at each peak was 20-30 s. The result of most analyses represents the averages of three or more individual spot analyses of feldspar, amphibole, and pyroxene. The representative analytical data, standards and the analytical error are listed in Tables 1, 2.

Major and trace element analysis of whole rock

A total of twelve samples, six from felsic, and six from mafic plutons were selected for major element and trace-element analysis of whole rock. The samples were analyzed by ICP-MS and XRF at Labwest Minerals Analysis in Australia using the method package group MAR04 and at Zarazma Mineral Studies Company in Iran, using the method package group MMS-01 and WR-01. The results are presented in Table 3.

Laser ablation ICP-MS dating

Table 4 reports the results of U-Pb analysis of zircons from three samples of felsic rocks of ALMC (f-86, f-84, f-60). Analysis was conducted using inductive laser ablation coupled with a plasma mass spectrometer (LA-ICP-MS) at the University of Adelaide (Australia). The zircons were separated using conventional methods that include crushing, sieving, magnetic separation, and floatation.

More than fifty zircon grains were handpicked under a binocular microscope. The zircons were set in synthetic resin mounts, polished, and cleaned in a warm HNO_3 ultrasonic bath. Equipment and operating conditions for zircon analysis were identical to those reported by Payne et al. (2006). A spot size of 30 μm and repetition rate of 5 Hz was used for U-Pb data acquisition, producing a laser power density of ~8 J/cm^2. Zircon age was calculated using the GEMOC GJ-1 zircon standard to correct for U-Pb fractionation (TIMS normalization

Table 1. Results of electron microprobe analysis (EPMA) of plagioclase and magnetite minerals in felsic rocks (Quartz-syenite, Syenogranite) of ALMC.

Sample No	f-51	f-51	f-51	f-84	f-84	f-84	f-84	f-84	f-51	f-84
Rock type	*quartz-syenite*			*syenogranite*					*quartz-syenite*	*syeno-granite*
mineral	*plagioclase*								*magnetite*	
SiO_2	67.07	68.9	68.58	69.15	64.39	64.26	64.68	64.04	0.21	0.31
TiO_2	0.00	0.00	0.01	0.00	0.00	0.02	0.00	0.00	0.02	0.08
Al_2O_3	20.34	19.38	20.13	19.77	18.33	17.8	17.72	17.85	0.02	0.04
FeO	0.05	0.08	0.04	0.06	0.00	0.00	0.01	0.03	99.49	99.59
MnO	0.01	0.00	0.00	0.00	0.00	0.00	0.00	0.02	0.14	0.00
MgO	0.00	0.00	0.00	0.00	0.00	0.00	0.00	0.00	0.01	0.00
CaO	0.07	0.04	0.07	0.03	0.00	0.00	0.02	0.05	0.00	0.00
Na_2O	10.22	10.81	11.55	11.38	1.52	0.2	1.163	0.43	0.00	0.00
K_2O	2.20	1.04	0.08	0.11	16.72	18.65	16.58	18.52	0.00	0.01
Total	99.96	100.25	100.45	100.50	100.96	100.93	100.17	100.94	100	100.04
Oxygens	8	8	8	8	8	8	8	8	4	4
Si	2.98	3	2.98	2.99	2.98	2.99	3	2.97	0.01	0.012
Ti	0.000	0.000	0.000	0.000	0.000	0.000	0.000	0.000	0.001	0.002
Al	1.030	1.000	1.030	1.010	0.990	0.970	0.960	0.990	0.001	0.002
Fe_2	0.000	0.000	0.000	0.000	0.000	0.000	0.000	0.000	2.915	2.91
Mn	0.000	0.000	0.000	0.000	0.000	0.000	0.000	0.000	0.006	0.000
Mg	0.000	0.000	0.000	0.000	0.000	0.000	0.000	0.000	0.001	0.000
Ca	0.003	0.002	0.003	0.001	0.000	0.000	0.001	0.003	0.000	0.000
Na	0.853	0.914	0.973	0.957	0.100	0.019	0.105	0.039	0.000	0.000
K	0.121	0.058	0.004	0.006	0.900	1.101	0.98	1.096	0.000	0.000
Sum	4.990	4.970	4.990	4.960	4.970	5.080	5.040	5.090	2.934	2.926
Ab	87.3	93.8	99.3	99.3	12.2	1.7	9.7	3.4		
An	0.3	0.2	0.3	0.1	0.0	0.0	0.1	0.3		
Or	12.4	6	0.4	0.6	87.8	98.3	90.2	96.3		

Standard Name	*Standard composition for electron microprobe analysis (EPMA)*
F on Fluorite	Fluorite = Ca: 51.33%, F: 48.67%
Na on Albite	Albite = Na: 8.77%, Al: 10.29%, Si: 32.13%, O: 48.81%
Mg on Periclase	Periclase = Mg: 60.30%, O: 39.70%
Al on Corundum	Corundum = Al: 52.92%, O: 47.08%
Si, Ca on Wollastonite	Wollastonite = Ca: 34.50%, Si: 24.18%, O: 41.32%
K on Orthoclase	Orthoclase = K: 14.05%, Al: 9.69%, Si: 30.27%, O: 45.99% ,
Ti on Titanite	Titanite = Ti: 100%
V on Vanadium	Vanadium = V: 100%
Cr on Chromite	Chromite = Cr: 68.42%, O: 31.58%
Mn on Rhodonite	Rhodonite = O: 37.72%, Mg: 0.98%, Si: 21.63%, Ca: 5.2%, Mn: 33.68%, Fe: 0.79%
Fe on Specularite	Specularite = Fe: 69.94%, O: 30.06%
Standard error: 2%	

Table 2. Results of electron microprobe analysis (EPMA) of pyroxene, amphibole, plagioclase, and ilmenite minerals in mafic rocks (Diorite, pyroxene-diorite) of ALMC.

Sample No	m-72	m-72	m-72	m-76	m-76	m-76	m-76	m-76	m-76	m-76	m-72
Rock type	*diorite*			*pyroxene-diorite*							*diorite*
mineral	*plagioclase*			*pyroxene*			*amphibole*			*ilmenite*	
SiO_2	53.47	54.80	54.11	56.52	56.24	56.65	44.43	46.17	43.83	0.05	0.08
TiO_2	0.09	0.05	0.08	0.65	0.75	0.12	0.51	0.38	0.40	48.16	48.08
Al_2O_3	30.50	28.67	30.29	0.78	1.03	1.70	13.16	12.52	12.96	0.02	0.11
FeO	0.28	0.22	0.32	10.02	10.02	11.27	18.08	16.96	17.64	49.08	48.94
MnO	0.00	0.00	0.00	0.26	0.27	0.22	0.29	0.25	0.23	2.60	2.70
MgO	0.00	0.00	0.01	17.19	16.71	15.96	7.81	8.04	7.84	0.10	0.10
CaO	12.08	11.91	12.03	13.39	14.48	12.66	12.94	13.16	13.90	0.00	0.01
Na_2O	3.85	4.29	3.37	0.51	0.00	0.45	0.00	0.00	0.34	0.00	0.00
K_2O	0.08	0.11	0.12	0.18	0.32	0.17	1.76	1.38	1.51	0.00	0.01
Total	100.35	100.05	100.33	99.50	99.82	99.20	98.98	98.86	98.65	100.01	100.03
Oxygens	8	8	8	6	6	6	23	23	23	3	3
Si	2.404	2.469	2.426	2.061	2.049	2.073	6.597	6.789	6.546	0.001	0.002
Ti	0.003	0.002	0.003	0.018	0.021	0.003	0.057	0.042	0.045	0.937	0.935
Al	1.616	1.523	1.601	0.034	0.044	0.073	2.304	2.17	2.282	0.001	0.003
Fe_2	0.011	0.008	0.012	0.306	0.305	0.345	2.245	2.086	2.203	1.062	1.058
Mn	0.000	0.000	0.000	0.008	0.008	0.007	0.036	0.031	0.029	0.057	0.059
Mg	0.000	0.000	0.000	0.934	0.907	0.870	1.728	1.762	1.745	0.004	0.004
Ca	0.582	0.575	0.578	0.523	0.565	0.496	2.059	2.074	2.224	0.000	0.000
Na	0.336	0.375	0.293	0.036	0.000	0.032	0.000	0.000	0.098	0.000	0.000
K	0.005	0.006	0.007	0.008	0.015	0.008	0.333	0.259	0.288	0.000	0.000
Sum	4.955	4.958	4.920	3.927	3.915	3.907	15.359	15.213	15.461	2.061	2.062

Standard Name	*Standard composition for electron microprobe analysis (EPMA)*
F on Fluorite	Fluorite = Ca: 51.33%, F: 48.67%
Na on Albite	Albite = Na: 8.77%, Al: 10.29%, Si: 32.13%, O: 48.81%
Mg on Periclase	Periclase = Mg: 60.30%, O: 39.70%
Al on Corundum	Corundum = Al: 52.92%, O: 47.08%
Si, Ca on Wollastonite	Wollastonite = Ca: 34.50%, Si: 24.18%, O: 41.32%
K on Orthoclase	Orthoclase = K: 14.05%, Al: 9.69%, Si: 30.27%, O: 45.99% ,
Ti on Titanite	Titanite = Ti: 100%
V on Vanadium	Vanadium = V: 100%
Cr on Chromite	Chromite = Cr: 68.42%, O: 31.58%
Mn on Rhodonite	Rhodonite = O: 37.72%, Mg: 0.98%, Si: 21.63%, Ca: 5.2%, Mn: 33.68%, Fe: 0.79%
Fe on Specularite	Specularite = Fe: 69.94%, O: 30.06%
Standard error: 2%	

data: $^{207}Pb/^{206}Pb$=608.3 Ma, $^{206}Pb/^{238}U$=600.7 Ma, and $^{207}Pb/^{235}U$=602.2 Ma) (Jackson et al., 2004) and Glitter software was used for data reduction (Van Achterbergh et al., 2001). Over the duration of this study, the reported average normalized ages for GJ-1 were 609±10 Ma, 600.2±2.7 Ma, and 601.9±2.4 Ma for the $^{207}Pb/^{206}Pb$,

Table 3. Representative major (wt%) and trace element (ppm) compositions of selected intrusive rocks of ALMC. Major oxides analyzed by XRF; rare-earth element and trace element analyzed by ICP-MS.

Samples		f-51	f-60	f-84	f-54	f-86	f-85	m-69	m-72	m-75	m-76	m-73	m-77
Rock type		*quartz-syenite*	*quartz-syenite*	*syeno-granite*	*syeno-granite*	*syeno-granite*	*quartz-syenite*	*diorite*	*diorite*	*pyroxene-diorite*	*pyroxene-diorite*	*pyroxene-diorite*	*diorite*
		felsic rocks of ALMC						*mafic rocks of ALMC*					
Major oxides	Det. Lim.												
SiO_2	0.01	68.97	71.99	69.32	72.31	72.88	71.45	56.29	55.09	52.38	52.99	46.78	51.83
TiO_2	0.01	0.67	0.32	0.37	0.39	0.36	0.39	0.5	1.48	0.39	0.65	2.39	0.78
Al_2O_3	0.01	13.51	13.49	13.8	12.8	13.02	13.52	18.9	14.21	18.9	17.77	13.42	16.58
Fe_2O_3	0.04	6.11	5.23	4.23	5.89	4.23	4.49	5.4	12.58	4.5	6.41	18.16	8.11
MnO	0.01	0.13	0.03	0.07	0.03	0.07	0.07	0.09	0.18	0.11	0.13	0.19	0.14
MgO	0.01	0.31	0.22	0.29	0.24	0.26	0.29	3.54	2.75	3.24	3.05	5.04	6.18
CaO	0.01	0.37	0.32	1.56	0.21	0.25	0.32	10.61	8.73	12.44	10.81	9.01	10.84
Na_2O	0.01	4.18	4.1	4.77	4.47	5.25	3.78	2.09	3.05	2.83	3.47	2.78	3.12
K_2O	0.01	4.34	4.25	4.85	2.46	2.66	4.61	1.96	1.69	2.05	1.5	1.42	1.2
P_2O_5	0.001	0.13	0.04	0.05	0.05	0.05	0.06	0.1	0.11	0.06	0.1	0.15	0.12
Total		98.72	99.99	99.31	98.85	99.03	98.98	99.48	99.89	96.9	96.88	99.34	98.9
Rare-earth element (ppm)													
La	0.01	43	55	77	52.7	77	64.3	8	17	6	15	8.17	3.51
Nd	0.3	47.9	49.5	60.7	46.8	62.8	50	10.4	19.3	7.4	15	13.6	7.9
Gd	0.05	11.03	8.8	13.4	8.15	13.74	10.3	2.76	5.18	2.36	4.37	2.48	1.47
Yb	0.05	5.8	3.6	8	3.97	8.2	9.24	1.3	2.5	1.1	2.1	1.95	1.1
Ce	0.1	91	128	161	121	161	131	18	36	12	30	18.3	7.55
Sm	0.05	10.12	9.41	12.02	9.47	12.24	10.5	2.07	4.19	1.41	3.33	3.12	1.88
Tb	0.01	1.8	1.28	2.13	1.33	2.21	2.24	0.47	0.84	0.4	0.68	0.6	0.37
Er	0.03	11.39	6.77	16.06	4.01	16.54	9.43	2.42	5.01	2.08	4.18	2.11	1.23
Lu	0.01	0.77	0.47	0.98	0.57	1	1.35	0.18	0.33	0.15	0.29	0.3	0.17
Pr	0.02	10.94	12.4	16.24	12.8	16.41	14.1	1.93	3.97	1.17	3.04	3.17	1.77
Eu	0.02	1.91	0.9	1.19	0.86	1.22	0.99	0.82	1.24	0.77	1.16	0.81	0.56
Dy	0.05	10.16	6.38	12.81	7.53	13.22	14	2.27	4.54	1.95	3.79	3.55	2.19
Tm	0.01	1.29	0.74	1.9	0.68	2.09	1.49	0.24	0.52	0.2	0.45	0.32	0.19
Trace-element (ppm)													
Ba	1	439	85	176	43.6	172	76.1	0.7	1.3	0.5	1.1	182	33.3
Y	0.1	54.7	28.8	74.9	23.3	76.4	63.3	12.1	24.1	10.4	21	14.4	9.06
Th	0.2	7.25	30.81	31.89	33.6	32.72	30.4	1.6	4.22	1.41	2.23	4.18	1.42
Zn	1	84	11	17	7.2	17	12.2	66	102	69	68	65.6	24.9
V	8	20	12	16	4	16	8	99	579	99	163	478	93
Cs	0.1	0.5	1	1	0.4	1	0.3	1.1	1.3	0.7	1	0.8	0.3
Co	0.2	5.7	3.5	4	3.6	3.9	2.8	21.9	66.8	21.8	31.1	52.6	13.8
Rb	0.1	124	89	162	30.6	155	36.6	75	63	29	40	30.7	7
Zr	0.1	62	32	51	2	32	2	15	15	16	20	2	3
Pb	0.1	7	3	3	2.9	4	2.4	5	8	33	8	4.6	4.8

Table 3. ...Continued

Samples		f-51	f-60	f-84	f-54	f-86	f-85	m-69	m-72	m-75	m-76	m-73	m-77
Rock type		*quartz-syenite*	*quartz-syenite*	*syeno-granite*	*syeno-granite*	*syeno-granite*	*quartz-syenite*	*diorite*	*diorite*	*pyroxene-diorite*	*pyroxene-diorite*	*pyroxene-diorite*	*diorite*
		felsic rocks of ALMC						*mafic rocks of ALMC*					
Major oxides	Det. Lim.												
Trace- element (ppm)													
Cu	0.1	13	13	14	41	13	16.2	48	57	81	56	62.1	65.2
Cr	2	9	9	18	3	12	3	260	16	187	119	5	58
Sc	1	9.8	3.1	3.7	0	3.6	1	30.5	42.9	32.7	43.3	23	10
Li	0.1	2	7	7	4	7	2.9	28	43	35	25	45.5	18.7
Sr	0.5	59.1	20	18.9	4.4	17.5	8.5	313.6	212.8	348	304.7	89.6	82.7
Nb	0.1	24.86	30.74	34.33	32.7	35.66	35.8	7.2	9.8	4.4	9.1	1	1.3
Ni	0.1	2	14	5	27	5	5	73	7	50	33	7	21
Hf	0.1	1.69	1.08	1.54	0.06	1.01	0.11	0.55	0.7	0.6	0.84	0.14	0.18
Ta	0.1	1.02	1.29	1.5	1.01	1.47	0.84	0.66	0.66	0.68	0.68	0.81	0.81
Normalized rare-earth element to chondrite (Boynton, 1984)													
$(Eu)_N$		25.99	12.24	16.19	11.70	16.60	13.47	11.16	16.87	10.48	15.78	11.02	7.62
$(Sm)_N$		51.90	48.26	61.64	48.56	62.77	53.85	10.62	21.49	7.23	17.08	16.00	9.64
$(Gd)_N$		42.59	33.98	51.74	31.47	53.05	39.77	10.66	20.00	9.11	16.87	9.58	5.68
$Eu^*=\sqrt{(Sm)_N \times (Gd)_N}$		47.01	40.49	56.47	39.09	57.71	46.27	10.64	20.73	8.12	16.97	12.38	7.40
$(Eu/Eu^*)_N$		0.55	0.30	0.29	0.30	0.29	0.29	1.05	0.81	1.29	0.93	0.89	1.03
Normalized trace- element to primitive mantle (Sun and McDonough, 1989)													
$(Nb)_N$		34.87	43.11	48.15	45.86	50.01	50.21	10.10	13.74	6.17	12.76	1.40	1.82
$(Ta)_N$		24.88	31.46	36.59	24.63	35.85	20.49	16.10	16.10	16.59	16.59	19.76	19.76
$(Ti)_N$		3.09	1.48	1.71	1.80	1.66	1.80	2.31	6.83	1.80	3.00	6.59	3.60
$(Th)_N$		85.29	362.47	375.18	395.29	384.94	357.65	18.82	49.65	16.59	26.24	49.18	16.71
$(La)_N$		62.59	80.06	112.08	76.71	112.08	93.60	11.64	24.75	8.73	21.83	11.89	5.11
$(Sm)_N$		22.79	21.19	27.07	21.33	27.57	23.65	4.66	9.44	3.18	7.50	7.03	4.23
$(Lu)_N$		10.41	6.35	13.24	7.70	13.51	18.24	2.43	4.46	2.03	3.92	4.05	2.30
$(Gd)_N$		18.51	14.77	22.48	13.67	23.05	17.28	4.63	8.69	3.96	7.33	4.16	2.47
$Nb^*=\sqrt{(Th)_N \times (La)_N}$		73.07	170.35	205.06	174.14	207.71	182.96	14.81	35.05	12.04	23.93	24.18	9.24
$Ti^*=\sqrt{(Sm)_N \times (Tb)_N}$		19.49	15.85	23.11	16.21	23.75	22.15	4.50	8.57	3.43	6.87	6.25	3.81
$Ta^*=\sqrt{(Th)_N \times (La)_N}$		73.07	170.35	205.06	174.14	207.71	182.96	14.81	35.05	12.04	23.93	24.18	9.24
Definition of Nb/Nb*, Ta/Ta*, and Ti/Ti* Terms after Peters and Day (2014)													
Nb/Nb*		0.48	0.25	0.23	0.26	0.24	0.27	0.68	0.39	0.51	0.53	0.06	0.20
Ta/Ta*		0.34	0.18	0.18	0.14	0.17	0.11	1.09	0.46	1.38	0.69	0.82	2.14
Ti/Ti*		0.16	0.09	0.07	0.11	0.07	0.08	0.51	0.80	0.52	0.44	1.06	0.94
$(La/Sm)_N$		2.75	3.78	4.14	3.60	4.07	3.96	2.50	2.62	2.75	2.91	1.69	1.21
$(Gd/Lu)_N$		1.78	2.32	1.70	1.78	1.71	0.95	1.90	1.95	1.95	1.87	1.03	1.07

$^{206}Pb/^{238}U$, and $^{207}Pb/^{235}U$ ratios, respectively (n=24) (Figure 2 and Table 4).

Sample description

Felsic intrusive rocks are medium to fine-grained and whitish to light gray in color (Figure 3a). The main minerals are K-feldspar, plagioclase, and quartz.

K-feldspar with 45 to 60 vol.% mainly exists as subhedral to euhedral (Or=87-99) and scarcely as fine crystals. Perthite exsolution is common and graphic textures are frequently observed (Figure 3 b,c,d). Lath-shaped plagioclase is albite (Ab=95-99) with 20 to 25 vol.% and mainly polysynthetic twinning (Figure 3 b,c,d). Anhedral quartz with 20 to 28 vol.% mostly show undulose extinction (Figure 3 e,g). Mafic minerals, which constitute less than 5 % are mainly characterized by green hornblende (Figure 3f).

Common accessory minerals are titanite, magnetite, and zircon. Subhedral titanite exists with brown color and rhombic shape (Figure 3f). Opaque minerals are magnetite, which particularly is present as inclusions in main minerals (Figure 3 e,g,h).

The mineralogy of this intrusive indicates that the felsic intrusive rock mainly contains syenogranite and quartz-syenite. Location and rock type of six samples of felsic rocks that selected for the analyses are demonstrated in Table 5 and outcrop of selected samples are shown in Figure 1c.

The typical graphic texture shows that the crystallization felsic intrusive rock has occurred at low temperatures near to the eutectic point of quartz+K-feldspar. The deficiency of extensive contact metamorphism around the felsic intrusive rock confirms the low-temperature cooling of the granite magma.

Mafic intrusive rocks are gray to dark gray and generally medium-grained (Figure 4a). The main minerals of these rocks are plagioclase, pyroxene, and amphibole.

Lath-shaped plagioclases with 40 to 60 vol.% are subhedral to euhedral and contain An=13-28, Ab=70-84, and Or<2.1 (Figure 4 b,c). Clinopyroxene with 10 to 38 vol.% consists of augite (Wo=23-53, En=42-58, and Fs=23-44) frequently substituted with amphibole along its rims (Figure 4 d,e,f). Subhedral amphibole with 12 to 25 vol.% has a ferro-hornblende to tschermakite composition. Also, it contains less than 5 vol.% quartz and K-feldspar. The texture is granular and intergranular (Figure 4 d,e,f).

Secondary minerals of mafic rocks include epidote and chlorite and opaque mineral is ilmenite (Figure 4 b,c,d). This mineralogy indicates that the mafic rocks of ALMC are mainly diorite and pyroxene diorite. Location and rock type of six samples of mafic rocks selected for the analyses are demonstrated in Table 5 and outcrop of the selected samples is shown in Figure 1c.

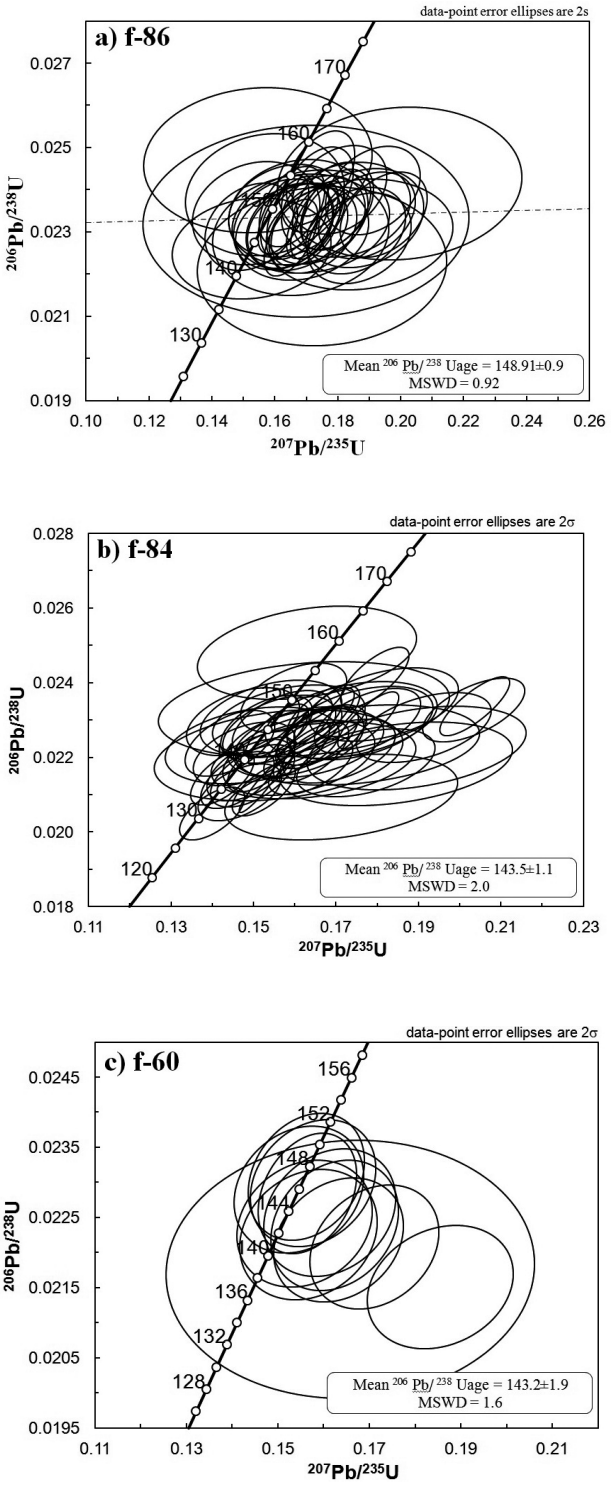

Figure 2. Zircon U-Pb concordia diagram of felsic rocks of ALMC, a) syenogranite (f-86); b) syenogranite (f-84); c) quartz-syenite (f-60).

Table 4. U-Pb LA-ICP-MS data of the felsic rocks of ALMC.

	Isotopic Ratios						Ages			
Analysis	$^{207}Pb/^{235}U$	1σ error	$^{206}Pb/^{238}U$	1σ error	err. corr.	Concordancy	$^{207}Pb/^{206}Pb$	1σ error	$^{206}Pb/^{238}U$	1σ error
f- 84 (syenogranite)										
f84-1	0.79427	0.01117	0.02675	0.00036	0.96	6	2946.5	19.49	170.2	2.24
f84-2	1.17212	0.01843	0.02964	0.00043	0.92	6	3400.6	23.25	188.3	2.69
f84-3	0.43618	0.00623	0.0238	0.00031	0.91	7	2137.3	21.28	151.6	1.98
f84-4	0.20883	0.00296	0.02257	0.00029	0.91	17	841.4	24.62	143.9	1.85
f84-6	0.6298	0.00824	0.0259	0.00033	0.97	6	2618.9	17.33	164.9	2.1
f84-8	0.50948	0.01018	0.02548	0.00038	0.75	7	2288	33.69	162.2	2.4
f84-9	0.23308	0.00642	0.02263	0.00034	0.55	14	1061	54.42	144.2	2.16
f84-10	0.23621	0.00392	0.02208	0.0003	0.82	12	1136.3	29.7	140.8	1.87
f84-11	0.22033	0.0047	0.02178	0.00031	0.67	14	1024.8	41.24	138.9	1.95
f84-12	0.35589	0.00561	0.0226	0.00031	0.87	8	1868.1	25.47	144	1.93
f84-13	0.15176	0.00215	0.02121	0.00028	0.93	48	280.9	27.01	135.3	1.74
f84-14	0.65453	0.00863	0.02556	0.00033	0.98	6	2705.2	17.48	162.7	2.08
f84-15	0.20365	0.00348	0.02337	0.00032	0.80	21	715.4	32.14	148.9	2
f84-16	0.2385	0.00473	0.02359	0.00033	0.71	15	1023.8	37.21	150.3	2.09
f84-17	0.44242	0.00634	0.02536	0.00034	0.94	8	2050.5	20.73	161.5	2.13
f84-18	0.16718	0.00299	0.02311	0.00031	0.75	48	306.1	36.25	147.3	1.98
f84-19	0.27279	0.00477	0.02384	0.00033	0.79	12	1269.7	30.59	151.9	2.07
f84-20	1.21842	0.01776	0.03247	0.00045	0.95	6	3318.7	19.51	206	2.79
f84-22	0.37448	0.0061	0.02513	0.00035	0.86	9	1767.8	26.29	160	2.17
f84-23	0.17782	0.00299	0.02299	0.00031	0.80	32	456.4	32.48	146.5	1.96
f84-24	0.16362	0.00322	0.02262	0.00031	0.70	47	306.1	41.03	144.2	1.97
f84-25	0.1669	0.00365	0.02315	0.00032	0.63	49	298.6	46.52	147.5	2.04
f84-26	0.7411	0.01289	0.02698	0.0004	0.85	6	2820	26.86	171.6	2.5
f84-27	0.16052	0.00325	0.02221	0.00031	0.69	47	304	42.48	141.6	1.94
f84-28	1.08511	0.01657	0.0305	0.00043	0.92	6	3234.9	21.41	193.7	2.69
f84-29	0.15855	0.00758	0.02299	0.00039	0.35	74	197.1	108.59	146.5	2.46
f84-30	0.17529	0.01207	0.02233	0.00044	0.29	29	489.2	147.79	142.4	2.76
f84-31	0.16265	0.00771	0.02238	0.00038	0.36	45	317.9	105.4	142.7	2.42
f84-32	0.14	0.00322	0.02049	0.00029	0.62	75	175	51.31	130.8	1.84
f84-33	0.15181	0.00331	0.0218	0.0003	0.63	63	219.9	47.67	139	1.92
f84-34	0.34689	0.00851	0.02306	0.00037	0.65	8	1785.7	44.7	146.9	2.31
f84-35	0.16452	0.01012	0.02192	0.00042	0.31	36	390.7	134.44	139.8	2.66
f84-36	0.19228	0.01111	0.02131	0.00042	0.34	17	789.9	119.25	135.9	2.65
f84-37	1.26325	0.03309	0.02828	0.00062	0.84	5	3589.6	45.94	179.8	3.9
f84-38	0.23344	0.01114	0.02215	0.00042	0.40	13	1107.4	94.99	141.3	2.68
f84-39	0.15555	0.00314	0.02262	0.00033	0.72	76	189.2	42.44	144.2	2.06
f84-40	0.16543	0.00411	0.02253	0.00034	0.61	42	339.5	53.32	143.7	2.15
f84-41	0.18453	0.01154	0.02183	0.00046	0.34	21	649.9	131.45	139.2	2.9
f84-42	0.53199	0.01654	0.02552	0.00049	0.62	7	2359.8	54.64	162.4	3.11
f84-43	0.20339	0.00507	0.02327	0.00035	0.60	21	721.3	50.23	148.3	2.23

Table 4. ... Continued

	Isotopic Ratios						Ages			
Analysis	$^{207}Pb/^{235}U$	1σ error	$^{206}Pb/^{238}U$	1σ error	err. corr.	Concordancy	$^{207}Pb/^{206}Pb$	1σ error	$^{206}Pb/^{238}U$	1σ error
f- 84 (syenogranite)										
f84-44	0.96714	0.01478	0.02949	0.00042	0.93	6	3106.1	20.01	187.3	2.61
f84-45	0.15316	0.00452	0.02281	0.00035	0.52	109	133.9	66.49	145.4	2.22
f84-46	0.15619	0.00561	0.02275	0.00037	0.45	78	185.8	81.15	145	2.33
f84-47	0.25968	0.00725	0.02255	0.00038	0.60	11	1281.8	53.71	143.7	2.38
f84-48	0.14965	0.00862	0.02233	0.00042	0.33	110	129.6	131.61	142.3	2.64
f84-49	0.14974	0.00418	0.0215	0.00034	0.57	63	218.4	62.07	137.2	2.12
f84-50	0.15698	0.00496	0.02289	0.00037	0.51	80	183.3	71.31	145.9	2.3
f84-51	0.16221	0.01439	0.02329	0.00052	0.25	68	218.9	195.63	148.4	3.26
f84-52	0.42416	0.00898	0.02463	0.00038	0.73	8	2027.2	35.81	156.9	2.41
f84-53	0.14912	0.00426	0.02166	0.00034	0.55	72	192.3	63.94	138.1	2.13
f84-54	0.16394	0.00372	0.02213	0.00033	0.66	39	359.9	47.86	141.1	2.05
f84-56	0.22434	0.00408	0.02383	0.00034	0.78	17	876.8	33.21	151.8	2.14
f84-57	0.17723	0.00685	0.02185	0.00037	0.44	25	561.2	82.59	139.3	2.35
f84-58	0.1758	0.00721	0.02292	0.0004	0.43	33	437.3	89.43	146.1	2.5
f84-59	1.09351	0.01954	0.02785	0.00044	0.88	5	3389.2	26.61	177.1	2.76
f84-60	0.41735	0.01453	0.02445	0.00047	0.55	8	2011.6	62.71	155.7	2.95
f84-61	0.16101	0.00753	0.02199	0.00041	0.40	42	333.8	103.87	140.2	2.56
f84-62	0.17765	0.00528	0.02296	0.00036	0.53	32	456.9	63.83	146.3	2.27
f84-63	0.19132	0.0067	0.0228	0.00038	0.48	23	634.5	73.76	145.3	2.4
f84-64	0.36212	0.01351	0.02206	0.00048	0.58	7	1942.3	69.42	140.7	3
f84-65	0.28447	0.09785	0.02326	0.00307	0.38	11	1397.9	577.53	148.2	19.36
f84-66	0.20943	0.00565	0.02286	0.00036	0.58	18	821	54.23	145.7	2.24
f84-67	0.21652	0.00476	0.02284	0.00034	0.68	16	891.1	42.43	145.6	2.14
f84-68	0.14777	0.00505	0.0221	0.00035	0.46	114	124.1	78.43	140.9	2.19
f84-69	0.27115	0.00702	0.02221	0.00035	0.61	10	1394.9	48.84	141.6	2.22
f84-70	0.17367	0.00852	0.02301	0.00042	0.37	37	401.8	107.37	146.7	2.62
f84-71	0.20447	0.0163	0.02151	0.0005	0.29	15	897.4	159.37	137.2	3.18
f84-72	0.26113	0.00818	0.02252	0.00038	0.54	11	1294.8	60.95	143.6	2.42
f84-73	0.18948	0.01086	0.02225	0.00046	0.36	21	666.7	121.02	141.8	2.88
f84-74	0.15611	0.0123	0.02205	0.0005	0.29	55	257	174.62	140.6	3.14
f84-76	0.33653	0.01183	0.02338	0.00046	0.56	9	1704.1	66.55	149	2.9
f84-77	0.16297	0.01087	0.02481	0.00051	0.31	195	80.9	154.56	158	3.19
f84-78	0.14745	0.00562	0.02296	0.00037	0.42	534	27.4	89.3	146.4	2.33
f84-79	0.33451	0.01667	0.02331	0.00051	0.44	9	1698.3	92.7	148.5	3.19
f84-80	0.17074	0.00558	0.02217	0.00035	0.48	32	446.4	71.11	141.4	2.22
f84-81	0.16387	0.00415	0.02178	0.00032	0.58	35	394.6	54.16	138.9	2.03
f84-82	0.18151	0.0074	0.02342	0.0004	0.42	32	460.1	89.75	149.2	2.54

Table 4. ... Continued

	Isotopic Ratios						Ages			
Analysis	$^{207}Pb/^{235}U$	1σ error	$^{206}Pb/^{238}U$	1σ error	err. corr.	Concordancy	$^{207}Pb/^{206}Pb$	1σ error	$^{206}Pb/^{238}U$	1σ error
f- 86 (syenogranite)										
f86-1	0.18053	0.00614	0.024	0.00043	0.31	39	394.5	72.06	152.9	2.69
f86-2	0.75175	0.01477	0.02862	0.00048	0.56	7	2746.9	28.22	181.9	3.03
f86-3	0.16983	0.02117	0.02325	0.00093	0.04	45	328	269.75	148.2	5.89
f86-4	0.16258	0.00645	0.02318	0.00044	0.24	63	234.8	88.92	147.7	2.8
f86-5	0.62154	0.01089	0.02836	0.00045	0.66	7	2444.9	23.19	180.3	2.83
f86-7	0.31679	0.00564	0.02502	0.00039	0.65	11	1463.9	26.51	159.3	2.48
f86-8	0.86098	0.02233	0.02926	0.00059	0.36	6	2931.6	42.11	185.9	3.67
f86-9	0.77785	0.01871	0.02897	0.00055	0.41	7	2782.8	38.29	184.1	3.42
f86-10	0.14271	0.02133	0.01786	0.00085	0.03	22	527.5	309.24	114.1	5.4
f86-12	0.15264	0.0103	0.02261	0.00049	0.13	99	146.1	152.55	144.1	3.08
f86-13	0.16742	0.00901	0.02347	0.00051	0.16	55	274.2	120.54	149.5	3.19
f86-14	0.16863	0.00865	0.023	0.00047	0.18	44	336	112.72	146.6	2.95
f86-15	0.16383	0.00756	0.0235	0.00045	0.21	68	221	103.33	149.7	2.86
f86-16	0.44116	0.01027	0.02507	0.00044	0.45	8	2065.8	38.18	159.6	2.78
f86-17	0.19112	0.00616	0.02398	0.00043	0.33	29	522.4	67.53	152.8	2.68
f86-18	0.16537	0.00425	0.0236	0.00039	0.43	65	232.7	54	150.4	2.47
f86-19	0.22638	0.00973	0.02376	0.00049	0.22	17	902.2	86.94	151.4	3.06
f86-20	0.36094	0.01056	0.02446	0.00046	0.35	9	1749.2	51.83	155.8	2.92
f86-21	0.31761	0.00669	0.02273	0.00038	0.54	9	1649	33.85	144.9	2.39
f86-22	0.18687	0.00673	0.02285	0.00044	0.28	25	578.8	75.83	145.6	2.74
f86-23	0.28763	0.00803	0.02503	0.00045	0.38	12	1276.8	51.45	159.4	2.8
f86-24	0.43334	0.00867	0.02591	0.00043	0.57	8	1975.5	30.29	164.9	2.7
f86-25	0.1793	0.00455	0.02353	0.00039	0.44	35	423	50.65	149.9	2.48
f86-26	0.1826	0.00833	0.02353	0.00046	0.21	32	462.6	98.82	149.9	2.9
f86-27	0.15248	0.00598	0.02312	0.00042	0.27	163	90.1	89.9	147.3	2.65
f86-30	0.22525	0.00477	0.02511	0.00041	0.55	21	776	37.97	159.9	2.57
f86-31	0.17134	0.01022	0.02324	0.0005	0.15	42	348.9	130.03	148.1	3.12
f86-33	0.19969	0.01588	0.02415	0.00074	0.08	26	602.9	169.95	153.8	4.68
f86-34	0.2384	0.00511	0.02405	0.00039	0.54	16	983.1	37.55	153.2	2.48
f86-35	0.18565	0.00648	0.02303	0.00042	0.30	27	547	72.97	146.8	2.64
f86-36	0.2826	0.00619	0.0244	0.00041	0.54	12	1293	36.92	155.4	2.58
f86-37	0.47679	0.01135	0.02628	0.00047	0.46	8	2119.7	38.34	167.2	2.96
f86-38	0.24497	0.00791	0.02351	0.00043	0.33	14	1083.9	61.68	149.8	2.72
f86-39	0.41407	0.00941	0.02495	0.00044	0.50	8	1962	36.47	158.9	2.75
f86-40	0.23336	0.00908	0.02355	0.00046	0.26	15	982.2	76.39	150.1	2.87
f86-41	0.29792	0.00911	0.02367	0.00044	0.35	10	1452.4	55.86	150.8	2.8
f86-42	0.27732	0.00861	0.02346	0.00044	0.34	11	1332.6	57.57	149.5	2.77
f86-43	0.2009	0.00604	0.02266	0.00041	0.37	19	751.9	59.65	144.4	2.56
f86-44	0.56211	0.01073	0.02672	0.00045	0.62	7	2374.9	26.8	170	2.82
f86-45	0.55027	0.02718	0.02597	0.00076	0.15	7	2387.2	88.53	165.3	4.75

Table 4. ... Continued

	Isotopic Ratios						Ages			
Analysis	$^{207}Pb/^{235}U$	1σ error	$^{206}Pb/^{238}U$	1σ error	err. corr.	Concordancy	$^{207}Pb/^{206}Pb$	1σ error	$^{206}Pb/^{238}U$	1σ error
f- 86 (syenogranite)										
f86-46	0.92855	0.01757	0.03023	0.00052	0.61	6	3001.2	25.46	192	3.23
f86-47	0.68884	0.01226	0.02774	0.00046	0.68	7	2654	22.86	176.4	2.86
f86-48	0.63768	0.01525	0.02648	0.0005	0.44	6	2602.7	37.95	168.5	3.15
f86-49	0.45238	0.00966	0.0254	0.00044	0.54	8	2087.1	32.88	161.7	2.75
f86-50	0.24379	0.00973	0.02364	0.00046	0.25	14	1062.8	77.85	150.7	2.91
f86-51	0.23328	0.00625	0.02387	0.00042	0.42	16	954.6	50.41	152	2.62
f86-52	0.29584	0.00747	0.02301	0.00041	0.45	10	1493	43.88	146.7	2.56
f86-53	0.2609	0.00547	0.02234	0.00037	0.56	11	1309.2	34.59	142.4	2.35
f86-54	0.17458	0.00445	0.02439	0.00041	0.44	55	281.9	52.71	155.3	2.58
f86-55	0.17847	0.00525	0.02362	0.00042	0.37	37	404.2	61.02	150.5	2.61
f86-56	0.18656	0.00604	0.02037	0.00038	0.32	16	819.9	65.06	130	2.41
f86-57	0.24687	0.01305	0.02378	0.00055	0.16	14	1076.5	105.13	151.5	3.46
f86-58	0.16268	0.00328	0.02341	0.00038	0.59	70	213.5	38.57	149.2	2.38
f86-59	0.18798	0.0079	0.02333	0.00048	0.23	27	546.7	89.99	148.6	3
f86-60	0.48592	0.01068	0.02626	0.00046	0.51	8	2153.5	34.52	167.1	2.86
f86-61	0.76134	0.06491	0.02853	0.00156	0.05	7	2772.4	153.5	181.4	9.76
f86-62	0.28746	0.00803	0.02438	0.00044	0.38	12	1327.1	51.23	155.3	2.77
f86-63	0.34316	0.01151	0.02462	0.00049	0.29	10	1644	61.1	156.8	3.06
f86-64	0.15398	0.00827	0.02344	0.0005	0.17	185	80.6	125.01	149.4	3.15
f86-66	0.90905	0.15162	0.02529	0.00223	0.02	5	3250.9	267.5	161	13.99
f86-67	0.175	0.01622	0.02218	0.00077	0.07	28	500	200.66	141.4	4.84
f86-68	0.18697	0.01211	0.02294	0.00054	0.13	26	571.2	137.5	146.2	3.41
f86-69	0.83133	0.15953	0.02469	0.00243	0.02	5	3147.8	304.46	157.2	15.27
f86-70	0.16826	0.01145	0.02293	0.00059	0.12	43	338.6	150.46	146.1	3.69
f86-71	0.5762	0.02157	0.02607	0.00064	0.22	7	2459.1	66.18	165.9	4.02
f86-72	0.17195	0.00334	0.02327	0.00037	0.61	42	354.5	35.31	148.3	2.36
f86-73	0.17348	0.00343	0.02328	0.00038	0.62	40	373.2	36.13	148.3	2.37
f86-74	0.23409	0.00543	0.02387	0.0004	0.50	16	961.2	41.92	152.1	2.53
f86-75	0.36724	0.00725	0.02419	0.0004	0.59	9	1801.4	29.91	154.1	2.52
f86-76	0.16725	0.00649	0.02311	0.00042	0.27	48	307.2	84.53	147.3	2.67
f86-78	0.22953	0.01012	0.02292	0.00046	0.22	15	1003.9	87.35	146.1	2.92
f86-80	0.16977	0.00449	0.02315	0.00039	0.43	44	336.7	54.42	147.6	2.47
f86-81	0.20519	0.0067	0.02316	0.00043	0.32	20	750.8	66.15	147.6	2.72
f86-84	0.15683	0.01033	0.02388	0.00059	0.13	188	80.7	153.61	152.1	3.73
f86-85	0.16506	0.00347	0.02287	0.00037	0.57	49	300.3	40.19	145.8	2.34
f86-86	0.16633	0.00443	0.02334	0.0004	0.44	55	271.7	55.48	148.7	2.49
f86-87	0.18927	0.00632	0.02339	0.00042	0.32	27	555.4	69.25	149.1	2.67

Table 4. ... Continued

	Isotopic Ratios						Ages			
Analysis	$^{207}Pb/^{235}U$	1σ error	$^{206}Pb/^{238}U$	1σ error	err. corr.	Concordancy	$^{207}Pb/^{206}Pb$	1σ error	$^{206}Pb/^{238}U$	1σ error
f-60 (quartz-syenite)										
f60-1	0.1613	0.00587	0.02257	0.00037	0.22	52	277.8	81.41	143.9	2.33
f60-2	0.16324	0.00577	0.02218	0.00036	0.23	41	344.7	78.16	141.4	2.28
f60-3	0.15588	0.00604	0.02241	0.00037	0.19	66	215.1	87.84	142.9	2.36
f60-4	0.31485	0.01004	0.02319	0.0004	0.23	9	1594.8	59.62	147.8	2.54
f60-5	0.18545	0.00652	0.02151	0.00036	0.22	20	691.5	74.08	137.2	2.3
f60-6	0.53974	0.01447	0.02582	0.00047	0.27	7	2363.7	47.16	164.4	2.95
f60-7	0.24222	0.00741	0.02299	0.00038	0.26	13	1105.3	60.22	146.5	2.37
f60-8	0.16584	0.01646	0.02176	0.00075	0.04	33	423	216.26	138.8	4.73
f60-9	0.15667	0.00613	0.02226	0.00038	0.19	59	242.1	88.7	141.9	2.42
f60-10	0.21693	0.00702	0.02345	0.00038	0.24	18	840	66.24	149.4	2.42
f60-11	0.15454	0.00579	0.0229	0.00037	0.21	101	144.9	85.81	146	2.35
f60-12	0.15624	0.00517	0.02308	0.00037	0.25	97	152.3	75.61	147.1	2.32
f60-13	0.17108	0.00578	0.02208	0.00036	0.24	31	458.8	73.66	140.8	2.26
f60-14	0.15648	0.0044	0.02284	0.00035	0.31	81	179.8	63.09	145.6	2.18
f60-15	0.36441	0.00876	0.02306	0.00037	0.34	8	1873.3	42.54	147	2.31
f60-16	0.16238	0.00568	0.02239	0.00038	0.22	46	310.7	78.37	142.8	2.37
f60-17	0.1577	0.00559	0.02299	0.00037	0.23	80	183.2	80.59	146.5	2.34

RESULTS

Whole-Rock Composition

The results of analysis of major and trace elements are listed in Table 3. There are two main components in the studied rocks; felsic rocks with high SiO_2 and Na_2O+K_2O located in the granite field and mafic rocks with low SiO_2 located in the quartz-diorite and diorite-gabbro field in the Middlemost (1994) diagram (Figure 5).

In Harker diagrams of felsic rock, Na_2O, K_2O, Rb, and Th show a positive trend with increasing SiO_2. The FeO_t, TiO_2, P_2O_5, CaO, MgO, Sr, and Eu contents of the rocks show a negative trend. These trends reveal differentiation of plagioclase and mafic minerals such as hornblende during magma crystallization, which follows normal crystal fractionation (Figures 6 and 13). These diagrams indicate that the two group's intrusions of ALMC are not contiguous. Each group shows some differentiation of elements with increasing SiO_2 (Figure 6). Decreasing trends for MgO, FeO_t, and TiO_2 are observed in the felsic and mafic rocks, but different trends for CaO and Al_2O_3 are observed in felsic and mafic rocks of ALMC.

According to Harker diagrams (Figure 6), the variation trend of main oxides in the felsic and mafic rocks of ALMC are similar to that of Suffi Abad intrusive samples (Azizi et al., 2011) and two samples (SH286 and SH257) studied by Shahbazi et al. (2015), respectively.

The diagram presented by Peccerillo and Taylor (1976) indicate the felsic rocks have high-K calc-alkaline affinity while the mafic rocks have a low-K calc-alkaline affinity (Figure 7). The felsic rocks of ALMC show more I-type granite and some A-type granite characteristics (Figure 8 a,b).

The behavior of REEs in the Sun and McDonough (1989) and Boynton (1984) spider diagrams (primitive mantle and chondrite) indicates that felsic rocks of the ALMC are enriched in the LREEs and LILEs (Figures 9a, 10a). The depletion of Eu, Ba, and Sr suggests plagioclase separation during differentiation or the presence of plagioclase in the source rock (e.g, Rollinson, 1993). In addition, the high content of Rb, Th, and in some samples, K and small percentages of Ti and Nb, suggesting the role of slab-derived fluid and the existence of minerals such as garnet and rutile in the source rock, which forms most of the arc magma (Plank and Langmuir, 1998; Becker et al., 2000) (Figure 9a).

The general abundance of REEs in mafic rock is lower than that in felsic rock; however, the Sun and McDonough (1989) diagram (primitive mantle) shows enrichment in some LILEs (e.g, Rb, Cs, and K) and a horizontal trend for HREEs and depletion of Nb, Zr, Ti, and P (Figures 9b, 10b). These chemical characteristics demonstrate concentrations of resistant minerals such as zircon and rutile in the

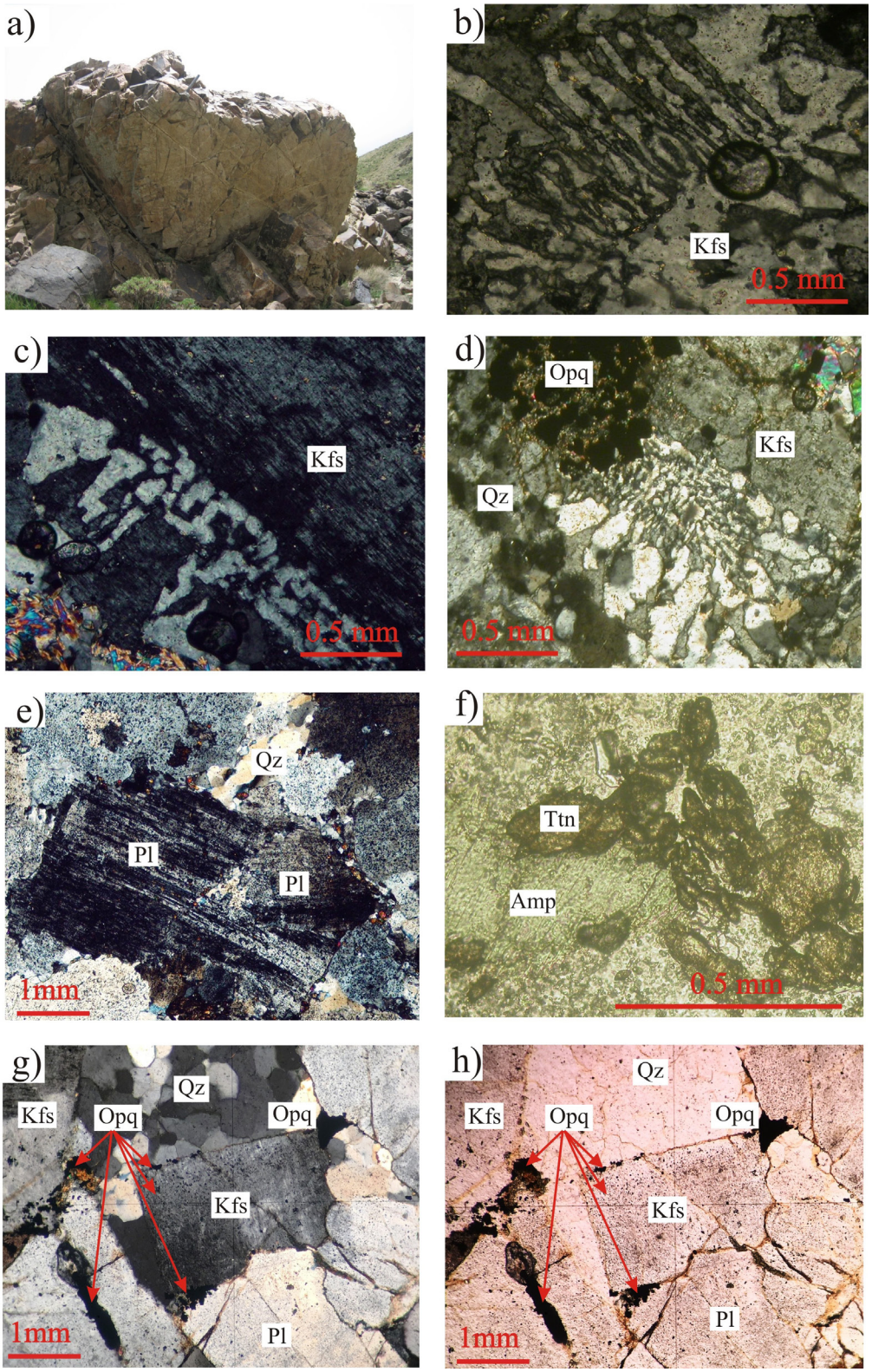

Figure 3. a) Field outcrops of felsic rocks (quartz-syenite, syenogranite) of ALMC; b,c) co-growths perthite, antiperthite and granophyric texture in XPL; d) granophyric texture and euhedral opaque minerals in XPL; e) opaque mineral inclusions in plagioclase and alkali feldspar in XPL; f) titanite with high relief and amphibole shown in PPL; g) it is shown inclusions of opaque minerals in plagioclase and alkali feldspar minerals of felsic rocks in XPL; h) in PPL (abbreviations from Whitney and Evans, 2010).

Table 5. The Rock type, locality, and GPS coordinates of selected samples of felsic and mafic rocks of ALMC.

Sample	*Rock group*	Location	Latitude Longitude	Rock name in petrological microscopy	Rock name in Middlemost (1994) diagram
f-51	*felsic rocks of ALMC*	South of the felsic pluton	34°50′55″ N 48°08′49″ E	Quartz-syenite	Granite
f-54		South of the felsic pluton	34°50′59″ N 48°08′27″ E	Syenogranite	Granite
f-60		South of the felsic pluton	34°51′20″ N 48°08′18″ E	Quartz-syenite	Granite
f-84		South of Posht dar band village	34°54′41″ N 48°07′40″ E	Syenogranite	Granite
f-85		South of Posht dar band village	34°54′51″ N 48°08′02″ E	Quartz-syenite	Granite
f-86		West of Baba Ali village	34°54′59″ N 48°09′16″ E	Syenogranite	Granite
m-69	*mafic rocks of ALMC*	West of the mafic pluton	34°53′48″ N 48°09′53″ E	Diorite	Quartz-diorite
m-72		West of Baba Ali village	34°55′36″ N 48°09′13″ E	Diorite	Quartz-diorite
m-73		West of Baba Ali village	34°55′18″ N 48°09′21″ E	Pyroxene-diorite	Diorite-gabbro
m-75		West of Baba Ali village	34°55′10″ N 48°10′52″ E	Pyroxene-diorite	Quartz-diorite
m-76		West of Baba Ali village	34°56′10″ N 48°10′15″ E	Pyroxene-diorite	Quartz-diorite
m-77		South of the mafic pluton	34°52′10″ N 48°10′37″ E	Diorite	Quartz-diorite

oceanic slab and precipitation of these minerals during magma crystallization. Some chemical parameters, such as the fluid in the subduction zone, play important role in the dissolution of HFSEs in the slab fluids. According to chondrite-normalized Boynton (1984), there is a flat pattern and some enrichment in LREEs and HREEs, and there is no enrichment in Eu (Figure 10b). In the discrimination diagrams of Pearce et al. (1984), the samples of mafic and felsic rocks of ALMC are classified as volcanic arc and with plate granite (Figure 11).

Geochronology

The U-Pb isotopic data are summarized in Table 4 and illustrated in Concordia diagrams (Figure 2 a,b,c). Three samples of felsic rock were analyzed (sample locations are shown in Figure 1c). Sample f-86 (34°54′59″ N, 48°09′16″ E) from west of Baba Ali, Sample f-84 (34°54′41″ N, 48°07′40″ E) from South of the Posht dar band village, and Sample f-60 (34°51′20″ N, 48°08′18″ E) from south of the felsic intrusive of ALMC were analyzed. The zircon from these samples is pink, prismatic, up to 300 μm in length, and perfectly euhedral. One hundred analyses of zircon from f-86 yielded a lower discordia intercept age of 148.91±0.9 Ma (95% confidence; MSWD=0.92) (Figure 2a; Table 4), 109 analyses of zircon from f-84 yielded a $^{206}Pb/^{238}U$ age of 143.5±1.1 Ma (95% confidence; MSWD=2.0) (Figure 2b; Table 4), and 16 analyses of zircon from f-60 yielded a weighted mean $^{206}Pb/^{238}U$ age of 143.2±1.9 Ma (95% confidence; MSWD=1.6) (Figure 2c, Table 4).

DISCUSSION

The felsic rocks of ALMC are either I-type or A-type granites

According to the following evidence, ALMC felsic intrusive rocks can be considered as I-type granites:

- The presence of amphibole and titanite and lack of muscovite and garnet;
- Placement of rock samples in Shand's diagram (Maniar and Piccoli, 1989) is in the peraluminous domain (Figure 12a);
- Chappell and White (1992) identified the array of I- and S-type granites in the Shand's diagram (Maniar and Piccoli, 1989) and reported that felsic rocks of ALMC granites are within the I-type zone (Figure 12a);
- Placement of rock samples in King et al. (2001)

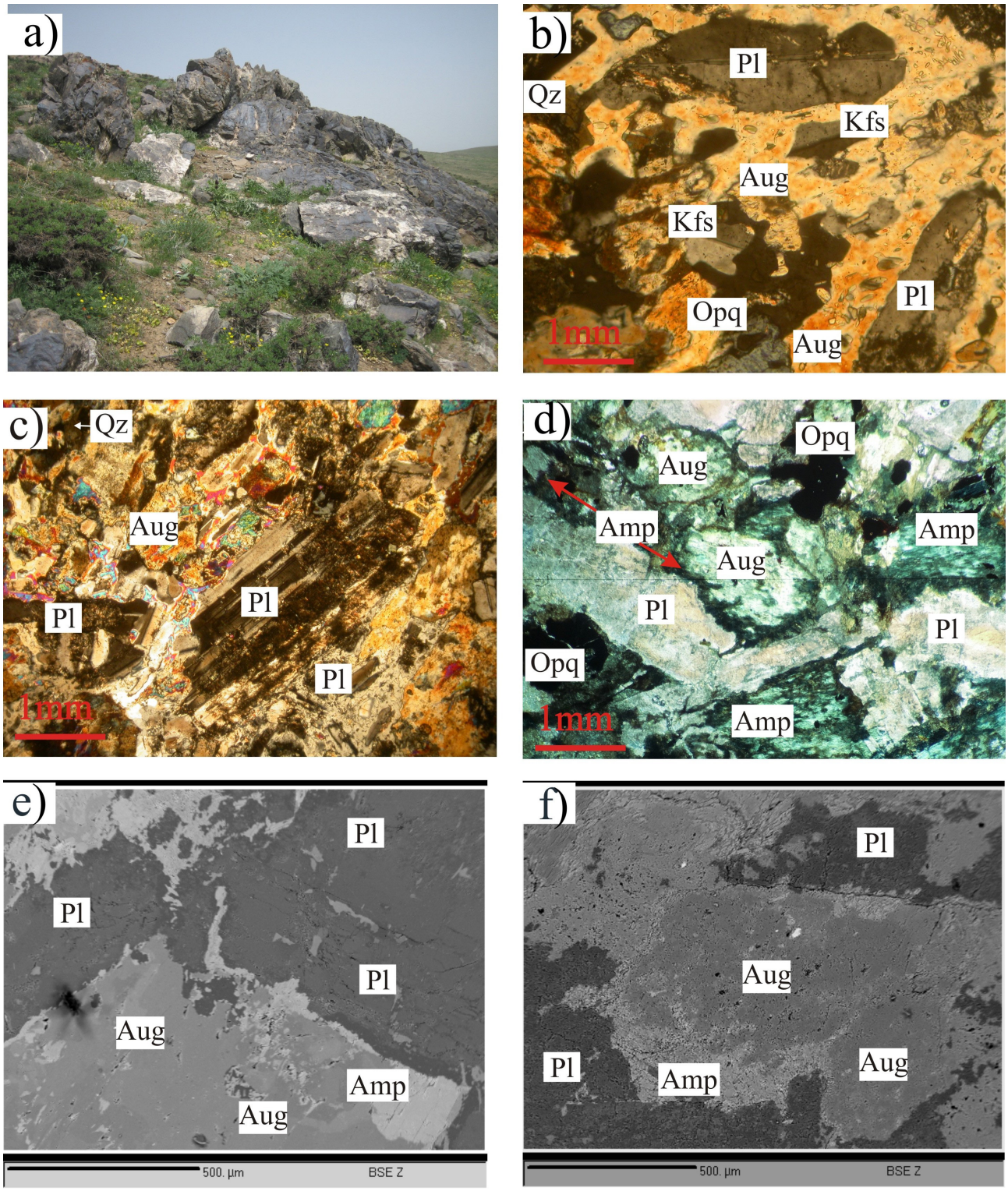

Figure 4. a) Field outcrops of mafic rocks (diorite, pyroxene-diorite) of ALMC; b, and c) lath-shaped plagioclase and k-feldspar are subhedral to euhedral with granular and inter granular textures; d) pyroxenes replaced by amphibole in the rim; e) BSE image of plagioclase, pyroxene, and amphibole; f) BSE image of pyroxenes replaced by amphibole in the rim (abbreviations from Whitney and Evans, 2010).

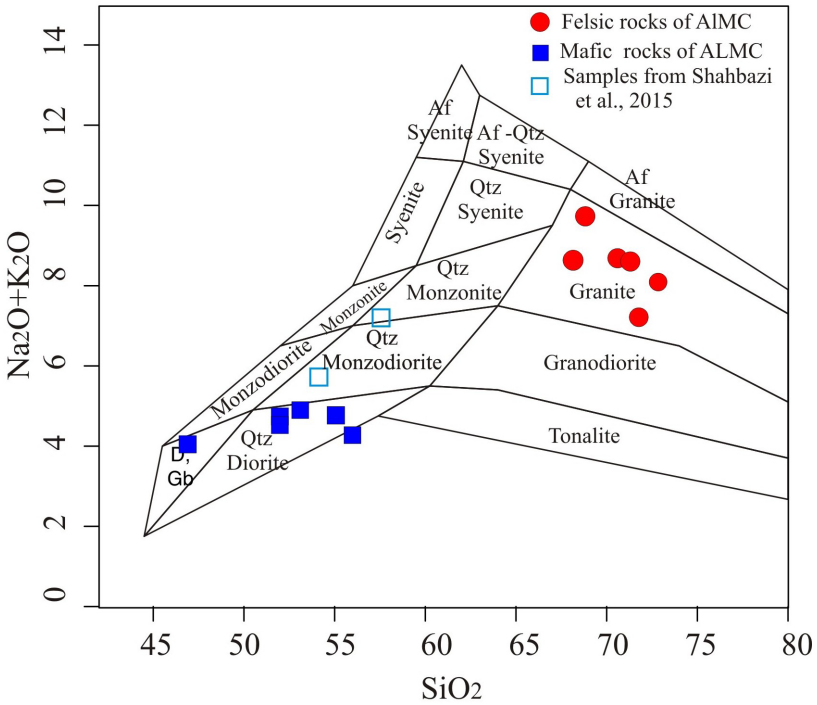

Figure 5. TAS diagram (Middlemost, 1994). Felsic rocks of ALMC plots on the granite fields and mafic rocks of ALMC plots on the quartz-diorite and diorite-gabbro fields, also two samples after Shahbazi et al. (2015) plots in the quartz-monzonite and quartz-monzodiorite.

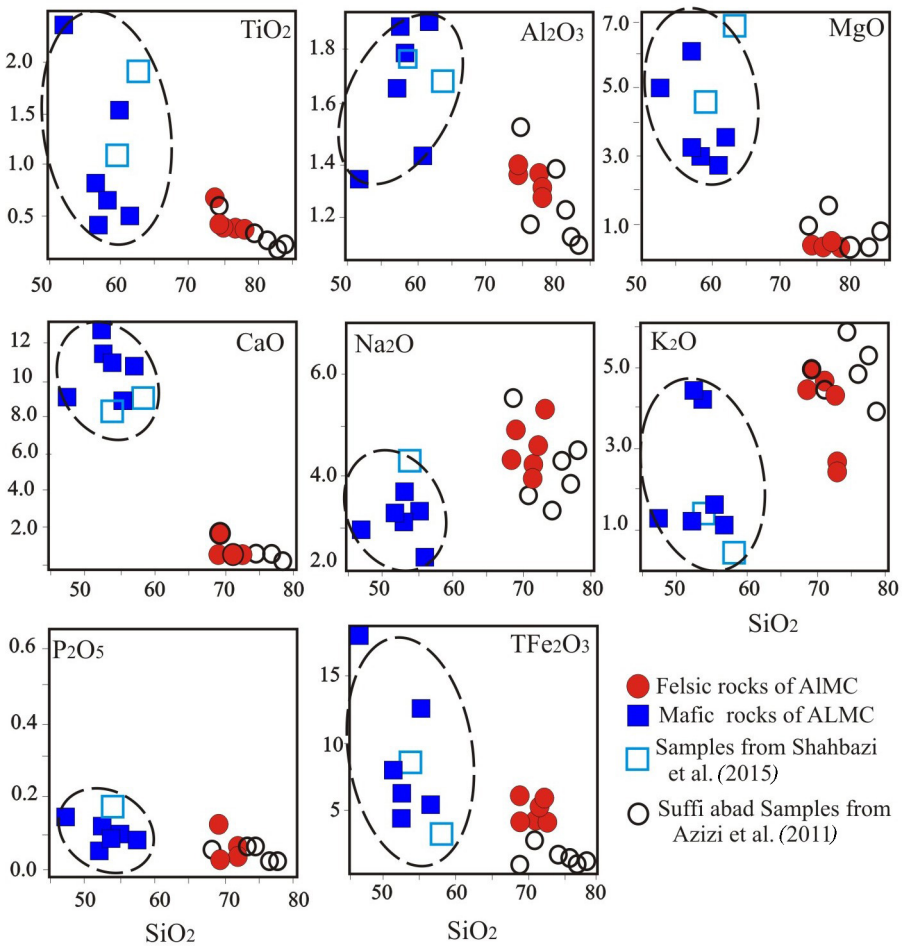

Figure 6. Selected Harker diagrams of felsic and mafic intrusive samples of ALMC, which is comparable to Suffi Abad intrusive samples after Azizi et al. (2011) and two samples after Shahbazi et al. (2015).

diagram in the I-type granites domain (Figure 12b);

- The ascending trend of Th vs SiO_2 that confirms I-type granite (King et al., 2001) (Figure 13a);
- The incremental trend of Rb vsY that confirms I-type granites (Figure 13f);

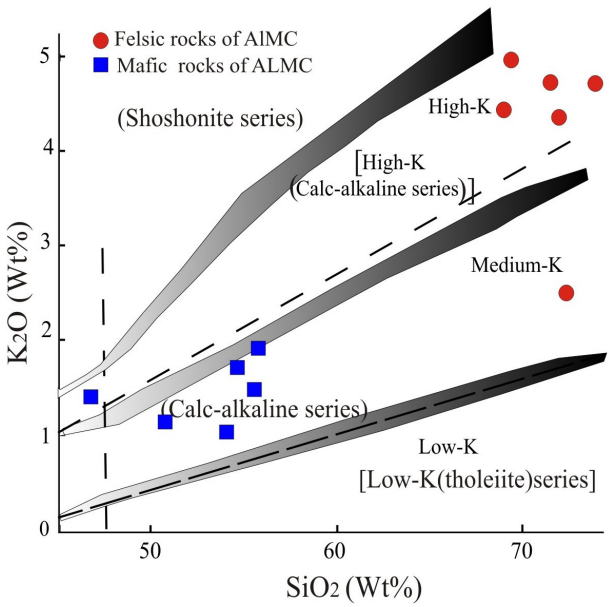

Figure 7. K_2O-SiO_2 diagram (Peccerillo and Taylor, 1976) subdivision after Le Maitre et al. (1989) and Rickwood (1989). Felsic rocks of ALMC plots on the high-K calc-alkaline field and mafic rocks of ALMC plots on calc-alkaline field.

- Placement of rock samples in Zn vs SiO_2 and Zr vs SiO_2 diagrams (Collins et al., 1982) in the I-type granites domain (Figure 14 a,b);
- Placement of the results of Nd-Sr isotope ratios presented by Amiri et al. (2017) in the I-type granites (Figure 15); and
- Saturation temperature of zircon (Watson and Harrison, 1983) is 512 °C to 675 °C, which suggests the presence of I-type granites temperature because the saturation temperature of zirconium for A-type granites is 800 °C higher than that of the other granite types (King et al., 2001; Badr et al., 2018).

However, based on the geochemical results, ALMC felsic intrusive rock has relatively A-type granite feature including:

- High concentrations of K_2O, Y, and Ce;
- Placing in Whalen et al. (1987) diagram at the boundary between I-type and A-type granites (Figure 8);
- Placing in the Y vs SiO_2 and Ce vs SiO_2 diagrams (Collins et al., 1982) between I-type and A-type granites (Figure 14 c,d); and
- Based on the new outcomes of Amiri et al. (2017), the felsic rocks of ALMC represent I-type and A-type dual features and are considered A-type granites because of the increase in Y, Ga, Ce, and Na_2O+K_2O contents and the decreased Ti, Sr, and Eu contents.

The magma series is one of the key parameters for granite type determination. In this regard, AlMC felsic intrusive rock is related to calc-alkaline magmatic series with high potassium (Figure 7) and confirms the I-type of

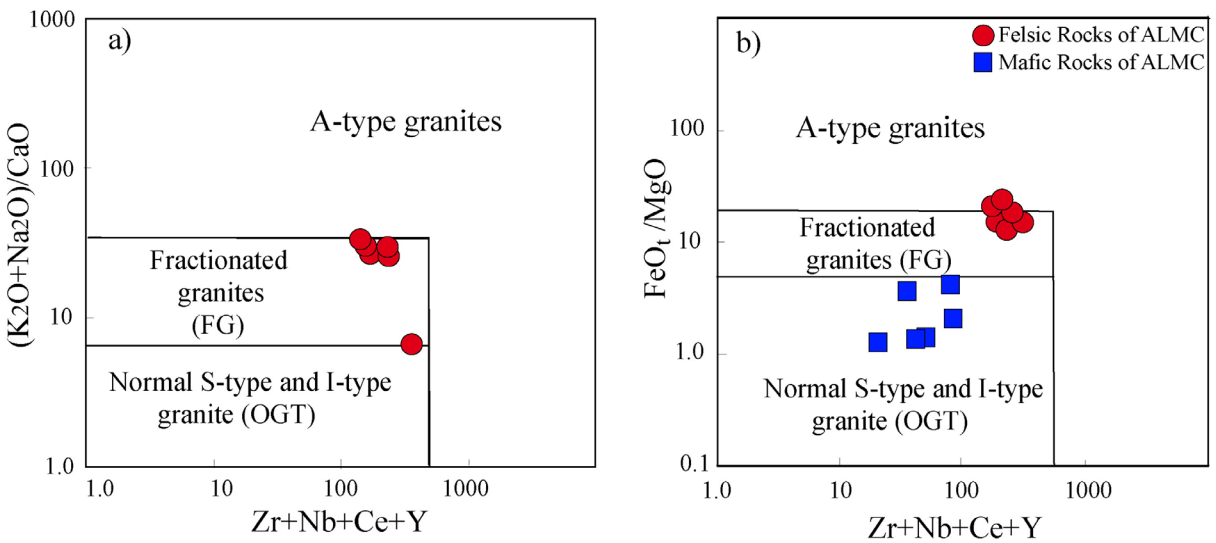

Figure 8. a) The (Na_2O+K_2O/CaO) vs Zr+Nb+Ce+Y (ppm) discrimination diagram of Whalen et al. (1987); b) the FeOt/MgO vs Zr+Nb+Ce+Y (ppm) discrimination diagram of Whalen et al. (1987), showing felsic and mafic intrusive samples separated from them. Mafic rocks lie in the normal array of granite and felsic rocks in the domain of fractionated granites and in the border area of fractionated granites and A-type granite.

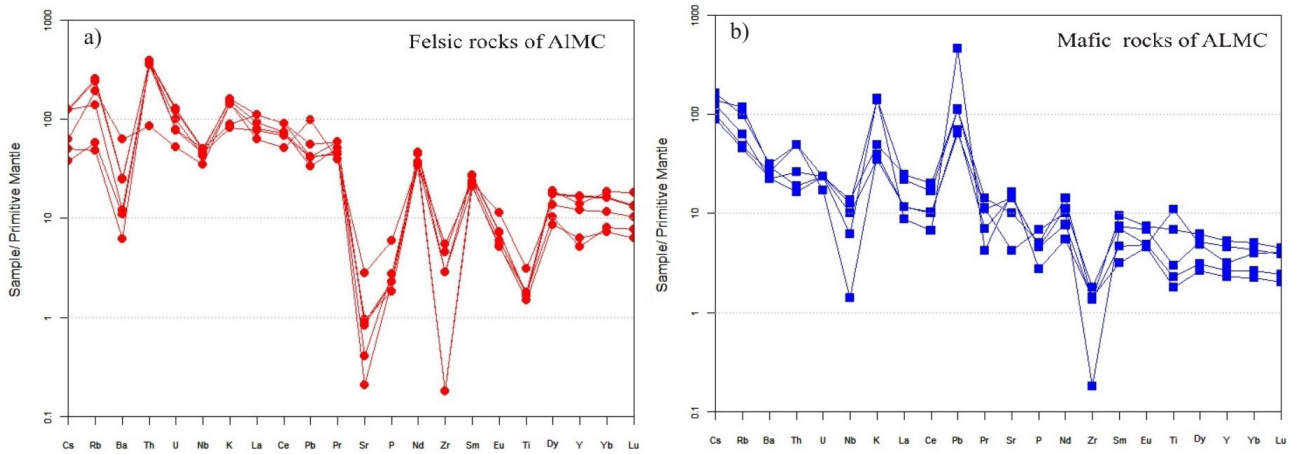

Figure 9. Primitive Mantle-Normalized spider diagram of felsic and mafic samples of ALMC (Sun and McDonough, 1989). a) Felsic rocks of ALMC; b) mafic rocks of ALMC.

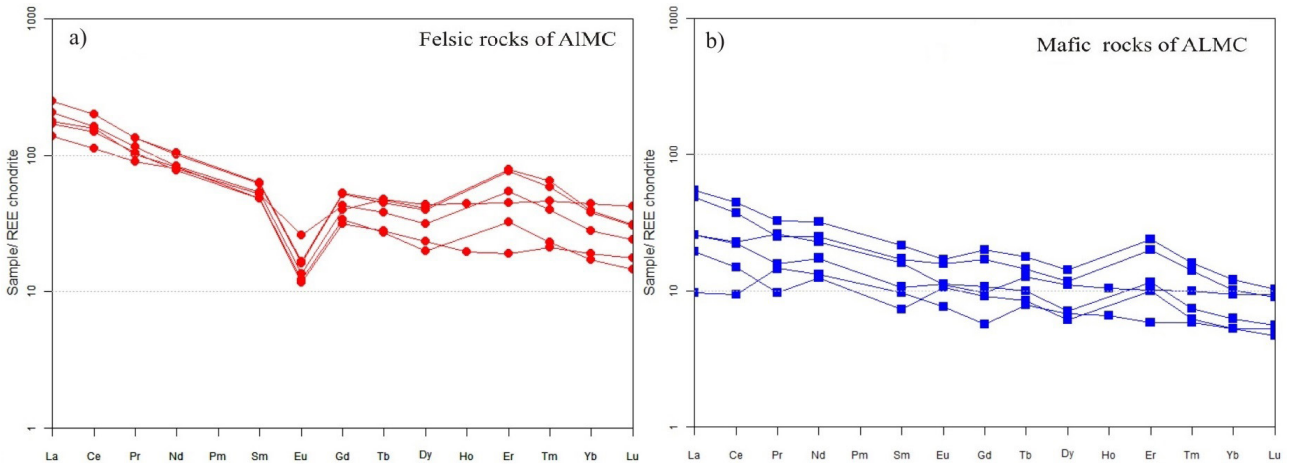

Figure 10. Chondrite-Normalized REE of felsic and mafic samples of ALMC (Boynton, 1984). a) Felsic rocks of ALMC; b) mafic rocks of ALMC.

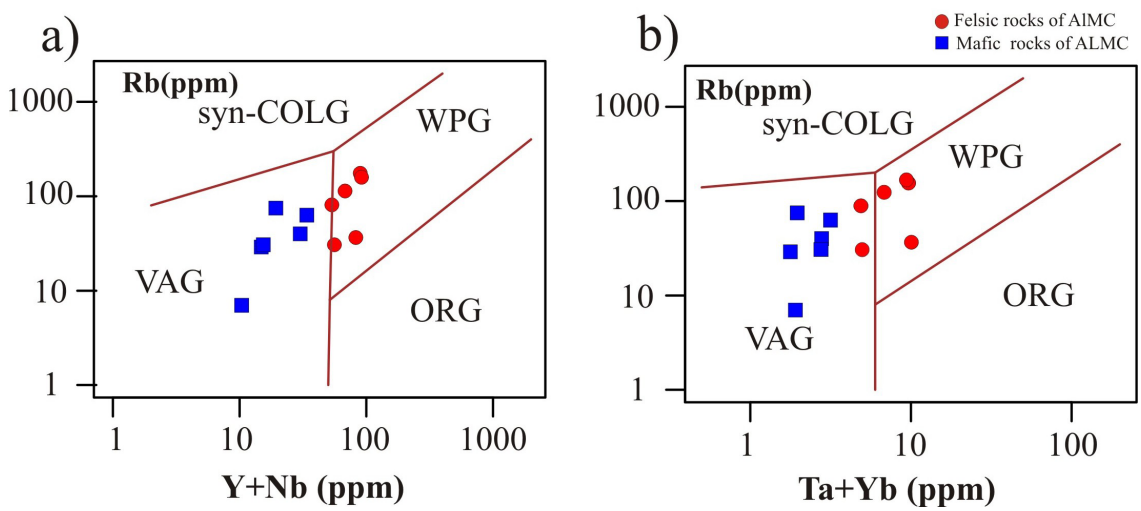

Figure 11. Discrimination of granite tectonic setting in diagram Pearce et al. (1984). a,b) show the mafic rocks of ALMC plot in the volcanic arc granite (VAG) and the felsic rocks of ALMC plots in the boundary of volcanic arc granite (VAG) and within plate granite (WPG).

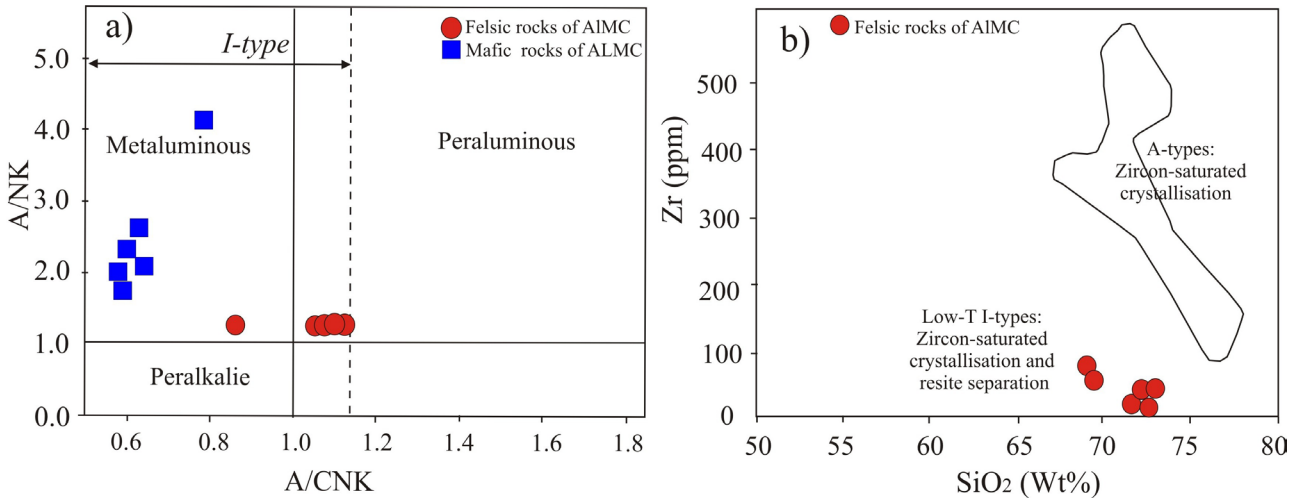

Figure 12. a) Shand's molar parameters A/NK vs A/CNK after Maniar and Piccoli (1989). Dashed line represents boundary between I- and S-type granites (Chappell and White, 1992); b) Zr vs SiO_2 diagram (King et al., 2001) for separation between the A-type and I-type granites.

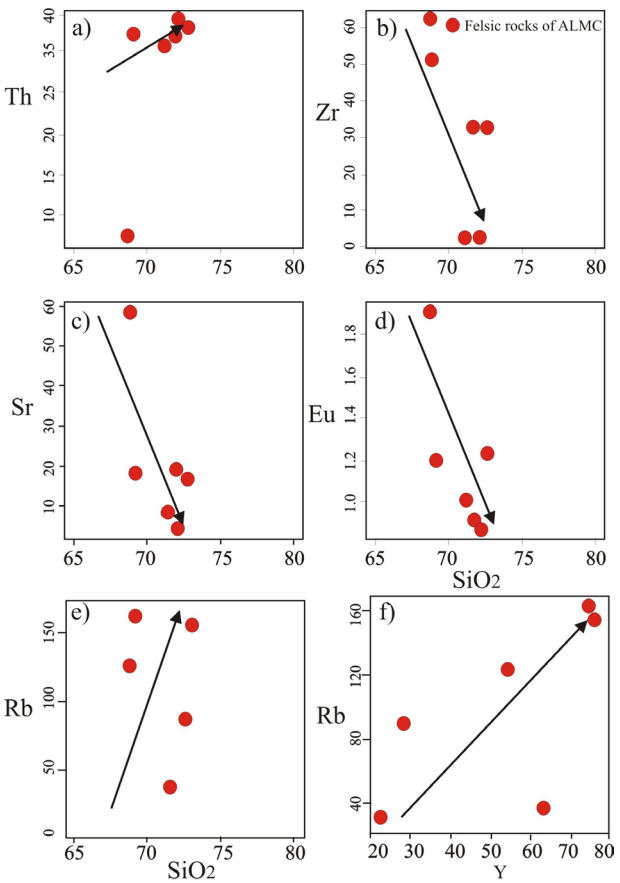

Figure 13. a) Th vs SiO_2 shows increasing trend; b) Zr vs SiO_2 shows decreasing trend; c) Sr vs SiO_2 shows decreasing trend; d) Eu vs SiO_2 shows decreasing trend; e) Rb vs SiO_2 shows increasing trend; f) Rb vs Y shows increasing trend.

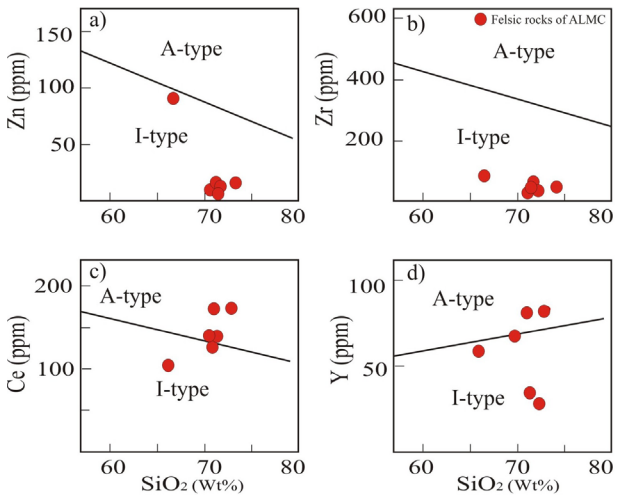

Figure 14. Harker variation diagrams for felsic rocks of ALMC; this shows the differentiation between A-type and I-type granites adopted after Collins et al. (1982). a) Zn vs SiO_2; b) Zr vs SiO_2; c) Ce vs SiO_2 and d) Y vs SiO_2.

ALMC granites.

Accordingly, AlMC felsic intrusive rock had I-type granites features. In the present study, due to the following reasons, AlMC felsic intrusive rock is considered as I-type granite:

1. Presence of amphibole and sphene in AlmC felsic intrusive rock;
2. Calc-alkaline magmatic series with high potassium; and
3. Most of the geochemical characteristics of this rock.

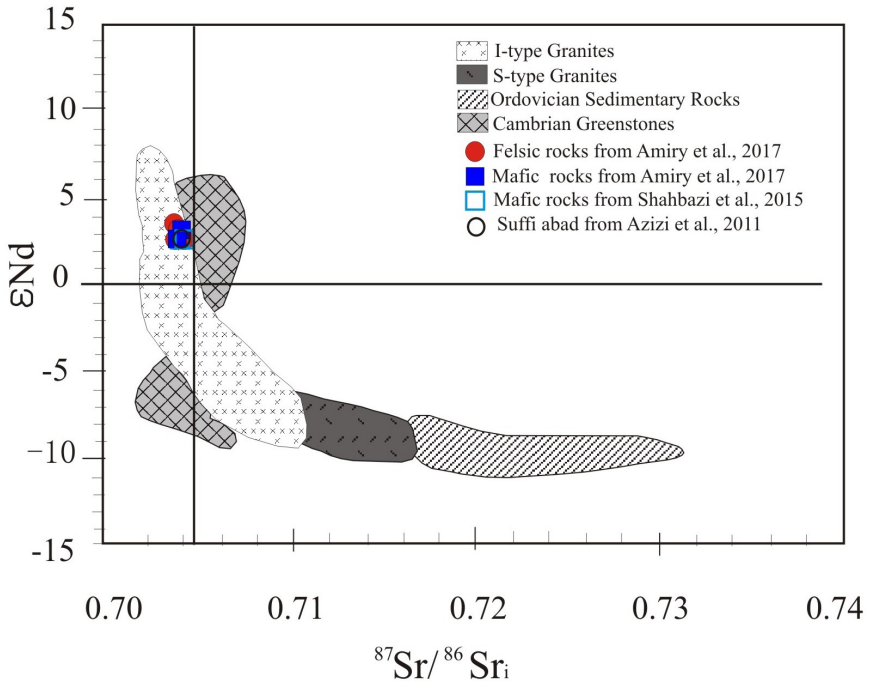

Figure 15. εNd vs $^{87}Sr/^{86}Sri$ diagram, the samples plot in the depleted mantle. mixing model modified after Keay et al. (1997); the isotopically primitive I-type granitoids, such as the Moruya Suite, are a mix of mantle (1) and partial melts from the Cambrian greenstone succession (2). These granitoids become variably contaminated with Ordovician metasediment (3) to generate the typical hyperbolic array of Lachlan Fold Belt granitoids.

Age of Intrusive rocks of ALMC

The late Jurassic to early Cretaceous (148-143 Ma) crystallization age of felsic rocks of ALMC was detected through more than 220 individual U-Pb analyses of zircon.

In Table 6, the age felsic intrusive of SSZ was collected (between 150 Ma to 140 Ma) for comparison with the felsic intrusion of ALMC. These intrusions consist of Suffi Abad (147.5±1.3 to 143.5±2.3 Ma according to Azizi et al., 2011) and Ghorveh and Galali with 147±3 Ma and 149±2 Ma, respectively (Yajam et al., 2015). The outcrop of these intrusions is shown in Figure 1b. The age of felsic intrusive rock of AlMC is same as that of Suffi Abad intrusive rock; therefore, the emplacement of these two intrusions in the SSZ is simultaneous.

Valizadeh and Zarian (1976) estimated the age mafic intrusive rock of AlMC 144±17 Ma by Rb-Sr methods based on the geochronology of total rock of diorite rocks. Moreover, the age of this mafic intrusive was reported to be 138-95 Ma by Shahbazi et al. (2015) who applied titanite U-Pb dating. Emplacement mafic intrusive rocks of SSZ mostly is related to late Jurassic (Hassanzadeh and Wernicke, 2016); for example, the emplacement of coarse-grained Kangareh (148.3±3.6 and 146.9±8.7 Ma, after Azizi et al., 2015) and Gorveh (149±0.2 Ma, after Mahmoudi et al., 2011) occurred on late Jurassic. In Table 7 the late Jurassic to early Cretaceous mafic intrusive rocks of SSZ and in Figure 1b the outcrops of these rocks are shown.

According to the results of reported dating for mafic rocks of ALMC by Valizadeh and Zarian (1976) and Shahbazi et al. (2015) mafic rock of AlMC is younger than the felsic rock of AlMC.

Frequency histogram of U-Pb zircon ages of igneous intrusion in SSZ reported by Hassanzadeh and Wernicke (2016) (Figure 16). In this ages histogram of SSZ igneous intrusion, five distinct groups were detected including Pan-African arc basement granites, Late Carboniferous-Early Permian rift-related "A-type" granites, Jurassic-Cretaceous Neotethyan arc batholiths, Late Cretaceous-Paleogene arc magmas, and Neogene collisional subvolcanic intrusions. The ages reported for ALMC intrusive are estimated using the histogram of Sanandaj-Sirjan intrusive rocks as the late Jurassic to early Cretaceous (Figure 16).

Magma sources and Tectonic setting

Mafic rocks of ALMC

The magma series of mafic intrusive rocks of ALMC are in calc-alkaline series and related to the subduction areas of island arc and have slight enrichment in LREEs ($(La/Sm)_N$=1.21-2.91) compared to the HREEs ($(Gd/Lu)_N$=1.03-1.95) (Table 3). The REEs shows that these rocks have a relatively low HREE Yb (1.1-2.5 ppm) and Y (9.06-24.1 ppm) (Figure 9b). Accordingly, and together with their relatively steep HREE patterns (Figure 10b), the residual phases of the source contain garnet and amphibole and/or pyroxene. They also have a relatively low Sr (Sr=82.7-348 ppm, <400ppm) content (Table 3) and

Table 6. Felsic intrusive rocks of SSZ that the emplacement age is the between 140 Ma and 150 Ma. The outcrop of this intrusive is shown in Figure 1b.

Area	Rock type	Dated mineral	Method	Age (Ma)	Interpretation	Reference	Rock types
Suffi Abbad	granite	zircon	U–Pb	143.5±2.3–147.5 ± 1.3	crystallization	Azizi et al. (2011)	felsic intrusive of SSZ
Ghorveh	undeformed monzogranite	zircon	U–Pb	147± 3	crystallization	Yajam et al. (2015)	
Galali	syenogranite	zircon	U–Pb	149± 2	crystallization	Yajam et al. (2015)	

Table 7. Mafic intrusive rocks of SSZ that the emplacement age is late Jurassic to early Cretaceous. The outcrop of this intrusive is shown in Figure 1b.

Area	Rock type	Dated mineral	Method	Age (Ma)	Interpretation	Reference	Rock types
Almogholagh	monazite (metamorphed and deformed)	titanite	U(Th)-Pb	95-138	crystallization	Shahbazi et al. (2015)	mafic intrusive of SSZ
Almogholagh	diorite	whole rock	Rb-Sr	144± 17	no data	Valizadeh and Zarian (1976)	
coarse-grained Kangareh (DKDJ-1)	gabbroic	zircon	U-Pb	148.3 ± 3.6	crystallization	Azizi et al. (2015)	
coarse-grained Kangareh (KMS-1)	gabbroic	zircon	U-Pb	146.9±8.7	crystallization	Azizi et al. (2015)	
Gorveh	gabbroic	zircon	U-Pb	149.3± 0.2	crystallization	Mahmoudi et al. (2011)	

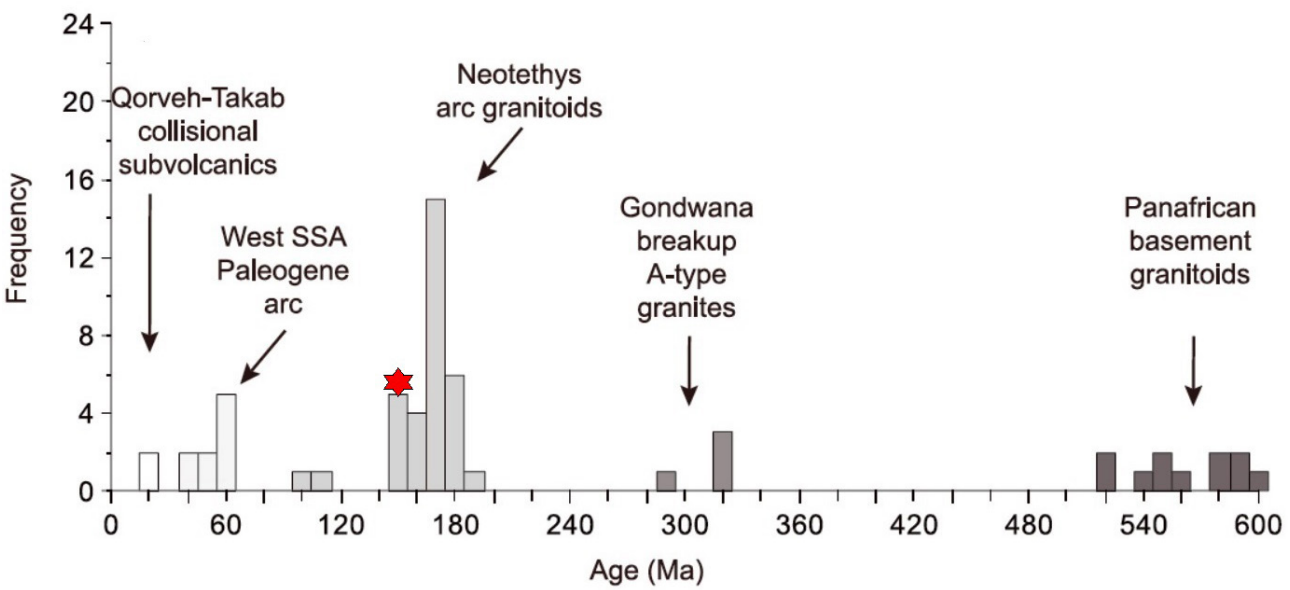

Figure 16. Showing felsic and mafic intrusives of ALMC on Frequency histogram of U-Pb zircon ages after Hassanzadeh and Wernicke (2016). Position of ALMC intrusive in Frequency histogram of U-Pb zircon ages is shown with red star.

show weak negative Eu (Eu/Eu*=0.81-1.29) anomalies (Figure 10b), suggesting melting the rock of a source in the plagioclase stability field (Wang et al., 2015). Hence, residual phases of the source of mafic rocks of ALMC containing garnet can be used to estimate the depth of the magma source (e.g., Jiang et al., 2013; Wang et al., 2015). The negative anomaly of Nb and Ti in the spider diagrams could indicate either the effect of fluids in a subduction zone or metasomatism of magma with the lower edge of the mantle (Sun and McDonough, 1989).

In Harker diagrams, mafic rocks are separated from felsic rocks of ALMC, as they are located in different positions. This observation is because of mafic oxides (Fe_2O_3, P_2O_5) reduction against increasing the SiO_2. This descending trend is due to the fractional crystallization of pyroxene and amphiboles in mafic rocks (Figure 6).

Mafic intrusive rocks of ALMC are different in terms of their geochemical and tectonic setting from the felsic intrusive rocks of ALMC (Figures 6 and 11). Since isotope data are used to determine the magma origin of intrusive rocks, we used the findings related to isotope data of ALMC rocks reported by Shahbazi et al. (2015) and Amiri et al. (2017) presented in Table 8.

The high Nd and low Sr ratios of isotopes for two samples (SH286 and SH257) reported by Shahbazi et al., (2015) in ALMC are $^{143}Nd/^{144}Nd$ (0.512605-0.512600) and $^{87}Sr/^{86}Sr$ (0.704610-0.705840), respectively. The positive ratio of εNd (+2.8-+2.7) approves that the depleted mantle of the subduction zone is the origin of mafic rocks of ALMC (Table 8).

Shahbazi et al. (2015) stated isotopic ratios of Sr and Nd of for intrusive rocks. Also, this author applied these isotopic data for determining the origin of magma of felsic and mafic intrusive rocks of ALMC. The outcomes related to the major oxides of SH286 and SH257 are shown in Figures 5 and 6. The rock sample SH286 and SH257 contain 54.00 and 58.00 SiO_2 respectively, and both samples have low K_2O content. Both mentioned samples are similar to the mafic rocks of ALMC. The geochemical findings are presented in Figures 5 and 6. Accordingly, isotopic ratios of Sr and Nd of SH286 and SH257 as well as titanite dating (Shahbazi et al., 2015) in this study were used to interpret the magma origin of mafic rocks of ALMC.

In addition, Amiri et al., (2017) reported the isotopic results of Sr and Nd in the mafic rocks of AlMC (Table 8). As can be seen from Table 8, AM-25, AM-46, and AM-47 samples are mafic rocks of AlMC with the low $^{87}Sr/^{86}Sr$ (0.705249, 0.704705, and 0.704422) and positive values εNd (+2.5,+2.3, and +3.3), respectively. These isotopic ratios indicate the depleted mantle origin mafic rocks of AlMC that are associated with subduction environments (Figure 15).

Based on the new scenario by Hassanzadeh and Wernicke (2016) that reviewing previous studies in SSZ, the emplacement of mafic intrusive rocks of ALMC is related to early Cretaceous rocks and subduction environments of an island arc.

Felsic rocks of ALMC

Felsic rocks of ALMC according to petrography (alkali feldspar and quartz simultaneously grow in the eutectic

Table 8. Rb-Sr and Sm-Nd isotopic data after Amiri et al. (2017) and Shahbazi et al. (2015) for mafic rocks of ALMC.

Sample	Rock group	Sr (ppm)	Rb (ppm)	$^{87}Rb/^{86}Sr$	$^{87}Sr/^{86}Sr$ (present)	$(^{87}Sr/^{86}Sr)$ (initial)	SiO_2	Reference	Rock types
AM-25	GD	451	3.20	0.021	0.705291	0.705249¶	54.78	Amiri et al. (2017)	mafic rocks of ALMC
AM-46	GD	357	18.7	0.152	0.705016	0.704705¶	49.73		
AM-47	GD	430	46.8	0.315	0.705066	0.704422	50.77		
SH286	monzodiorite	482.6	56.1	0.3362	0.705257	0.704610	54	Shahbazi et al. (2015)	
SH257	monzonite	418.8	6.2	0.0426	0.705921	0.705840	58		

Sample	Rock group	Nd (ppm)	Sm (ppm)	$^{147}Sm/^{144}Nd$	$^{143}Nd/^{144}Nd$ (present)	$(^{143}Nd/^{144}Nd)$ (initial)	$\varepsilon^{t}Nd$	SiO_2	Reference	Rock types
AM-25	GD	14.3	3.71	0.157	0.512730	0.512582¶	+2.5	54.78	Amiri et al. (2017)	mafic rocks of ALMC
AM-46	GD	17.6	5.05	0.174	0.512735	0.512572¶	+2.3	49.73		
AM-47	GD	9.10	2.09	0.139	0.512751	0.512620	+3.3	50.77		
SH286	monzodiorite	17.3	4.1	0.1451	0.512734	0.512605	+2.8	54	Shahbazi et al. (2015	
SH257	monzonite	30.4	7.3	0.1444	0.512728	0.512600	+2.7	58		

point) and saturation thermometer of zircon (Watson and Harrison, 1983) lower than 800 °C (it is 512 °C to 675 °C) suggest magma crystallization at a low temperature (King et al., 2001; Badr et al., 2018).

Moreover, these rocks present a low content of CaO, Al_2O_3, TiO_2, and MgO and high content of SiO_2 and Na_2O+K_2O. The low temperature of crystallization could be attributed to the highly viscous granitic magma that was crystallized in situ.

These rocks have high-K calc-alkaline magma series and their tectonic is related to the subduction area (Figure 7). The Ti (Ti/Ti*=0.07-0.16), Nb (Nb/Nb*=0.23-0.48), and Ta (Ta/Ta*=0.11-0.34) normalized to primitive mantle show ratios less than <1, so TNT (Ti, Nb, Ta) (Definition of Nb/Nb*, Ta/Ta*, and Ti/Ti* terms after Peters and Day, (2014)) anomalies are negative, which is the characteristic of subduction areas (Sun and McDonough, 1989) (Figure 9a and Table 3). LREEs ($(La/Sm)_N$=2.75-4.14) show an enrichment compared to the HREEs ($(Gd / Lu)_N$=0.95-2.32). The relative contents of Sr, Y and Yb in granitic rocks are estimated to find whether the granitoids are derived from the normal (~30-40 km) or thickened (>50 km) crust (e.g., Jiang et al., 2013; Wang et al., 2015). The felsic rocks of ALMC show a high Yb (Yb=3.6-9.24>1.9 ppm) and Y (Y=23.3-76.4>18 ppm) (Table 3), thus, we cannot consider garnet as a residual phase. Our results show a low of Sr (Sr=4.4-59.1<400ppm) and a negative Eu (Eu/Eu*=0.29-0.55) anomaly in the felsic rocks (Figure 10a and Table 3), suggesting the melting of a source rock of the felsic rocks of ALMC within the stability field of plagioclase.

Overall, petrography, zircon saturation thermometer, and geochemical considerations show that the source region of the felsic rocks of ALMC is located at a relatively shallow depth.

According to the isotopic data presented by Amiri et al. (2017) for 4 samples (AM-07, AM-23, AM-09 and AM-30), felsic rocks of ALMC have the isotopic ratio of $^{87}Sr/^{86}Sr$ (0.704484, 0.705825, 0.705769, and 0.705082) and positive value of εNd (+3.7, +3.2, +2.6, and +2.5) respectively (Table 9). The mantle can be considered as the origin of the felsic rocks magma and is associated with the subduction environments (Figure 15). Therefore, the isotope ratios and chemical composition do not confirm a crustal origin for the felsic rocks of ALMC. Moreover, Patiño Douce (1999) plots were applied to determine the origin of granites of ALMC divided based on different origins of granites and melt-forming pressure (Figure 17). In these diagrams, the chemical of formation felsic rocks of ALMC in term of pressure is at the low-pressure field (<4 kbar). Patiño Douce (1999) reported that pressure, particularly a low pressure, controls the composition of basaltic and andesitic-basaltic melt (4 kbar or less), the peritectic assemblage is dominated by Ca-rich plagioclase, and the melts are depleted in Ca and A1 relative to calc-alkaline granites (Patiño Douce,1999). Some factors such as a change in the depth and pressure in magma formation (Patiño Douce, 1999) as well as fugacity change in magma gases (Sisson et al., 2005) can be effective in magma formation of high-K calc-alkaline (e.g, Soesoo 2000; Ferré and Leake, 2001).

At pressures greater than 8 kbar, the peritectic assemblage is dominated by clinopyroxene±garnet, and the melts become too peraluminous compared to calc-alkaline rocks. At 8 kbar pressure, due to Ca-plagioclase crystallization, the melt would be poor in Ca, Al, and probably Eu (Patiño Douce, 1997, 1999). In comparison, because of clinopyroxene and garnet crystallization, it is

Table 9. Rb-Sr and Sm-Nd isotopic data after Amiri et al. (2017) for felsic rocks of ALMC.

Sample	Rock group	Sr (ppm)	Rb (ppm)	$^{87}Rb/^{86}Sr$	$^{87}Sr/^{86}Sr$ (present)	$(^{87}Sr/^{86}Sr)$ (initial)	SiO_2	Reference	Rock types
AM-07	QM	181	85.5	1.367	0.706892	0.704484¶	63.33	Amiri et al. (2017)	Felsic rocks of ALMC
AM-23	QM	282	56.2	0.577	0.706841	0.705825¶	67.52		
AM-09	QS	73.2	79.0	3.124	0.711274	0.705769¶	65.31		
AM-30	QS	49.6	80.8	4.72	0.713393	0.705082	64.96		

Sample	Rock group	Nd (ppm)	Sm (ppm)	$^{147}Sm/^{144}Nd$	$^{143}Nd/^{144}Nd$ (present)	$(^{143}Nd/^{144}Nd)$ (initial)	ε_{Nd}^{t}	SiO_2	Reference	Rock types
AM-07	QM	45.6	8.59	0.114	0.512762	0.512669¶	+3.7	63.33	Amiri et al. (2017)	Felsic rocks of ALMC
AM-23	QM	49.4	9.23	0.113	0.512733	0.152642¶	+3.2	67.52		
AM-09	QS	50.2	10.2	0.123	0.512711	0.512612¶	+2.6	65.31		
AM-30	QS	48.0	10.6	0.134	0.512713	0.512605¶	+2.5	64.96		

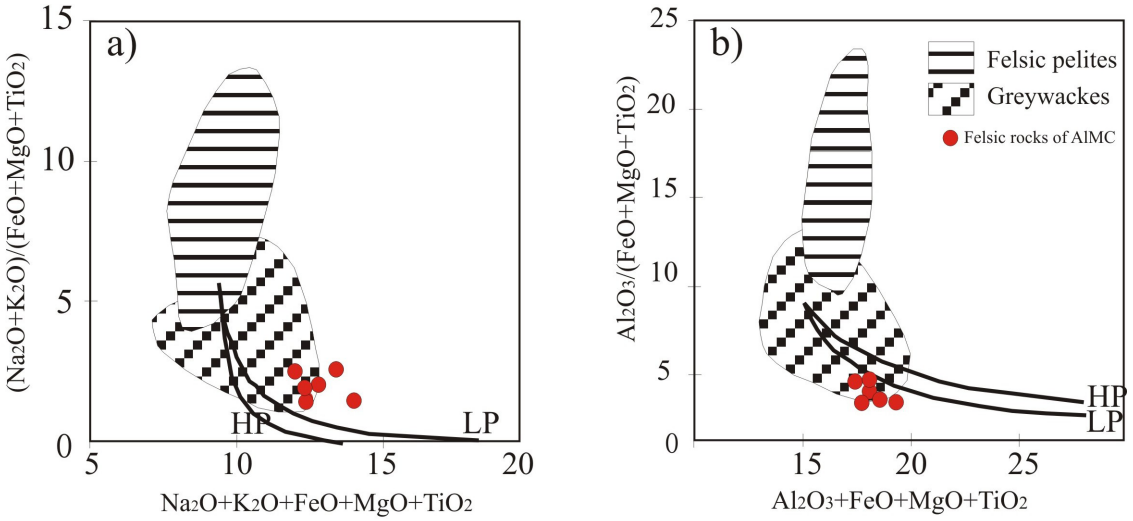

Figure 17. a,b) Composition of felsic rocks of ALMC in Patiño Douce (1999) diagrams for different sources of granite rocks. All samples are plotted in the greywacke field. LP and HP show the composition of melts at low pressure (<4 kbar) and high pressure (=8 kbar).

enriched by Al (Skjerlie and Johnston, 1993; Patiño Douce and Beard, 1995; Patiño Douce, 1997, 1999), which is the main component of peraluminous granite.

According to the felsic intrusive samples of ALMC in Patiño Douce (1999) diagram plot, at low pressures in the greywacke field (Figure 17), the formation of greywacke rocks is similar to that of andesite and basalt rocks (Patiño Douce, 1999). Thus, the origin granites of ALMC can be similar to the granites derived from basic or andesite magma at low pressure (Roberts and Clemens, 1993).

The formation of high-K calc-alkaline granites derived from basalt and andesite calc-alkaline magma is possible at the pressure lower than 4 kbar. These magmas show the depleted mantle origin (Azizi et al., 2011; Roberts and Clemens, 1993). However, according to the SiO_2 and MgO contents, the mantle cannot directly produce this magma. In this regard, the increasing trend of La/Sm vs La suggests the formation by melting process (Blein et al., 2001) (Figure 18). All these characteristics can be observed for felsic rocks of ALMC (Tables 3 and 9).

According to the new scenario of SSZ (Hassanzadeh and Wernicke, 2016), tectonic environment alteration of island arc and formation of back-arc basins in the period of early to late Cretaceous at the northern region of SSZ resulted in the generation of diverse A-type granites. In addition, some studies reported that arc-associated magmatic activity in the SSZ occurred in an extensional geodynamic location (Agard et al., 2005; Mohajjel et al., 2003; Alavi, 1994; Hassanzadeh et al., 2008). Also, changes in I-type calc-alkaline granitic intrusive rocks and their alteration to A-type alkaline granites in Ghorveh-Dehgolan and Dehgolan granites was presented by Sarjoughian et al. (2015) and Yajam et al. (2015), respectively. These observations at the northern SSZ confirm the changes in subduction environment (island arc) and formation of the back-arc basin in this area.

Therefore, considering petrography, geochemical, and isotopic data, we can attribute the formation of felsic intrusive magma of ALMC to the calc-alkaline andesite and basalt magma at the pressures lower than 4 kbar in subduction area; where its emplacement coincides with a change in tectonic environment at the northern SSZ. These changes have led to a condition in which felsic intrusive rocks of ALMC show mostly I-type and some A-type granite characteristics.

Comparing felsic intrusive rocks of ALMC with Suffi Abad intrusive rocks in SSZ

The emplacement of Suffi Abad intrusive rocks (Azizi et al., 2011) is the same as felsic intrusive rocks of ALMC at the late Jurassic until the early Cretaceous at the northern SSZ (Table 6).Consequently, the spider diagram presented in Figure 19 show similar trends and geochemical behaviour. In spider diagram, both rocks show negative anomalies in Ti, Zr, and Nb (Figure 19 a,b). In REEs diagram, both rocks show enrichment in LREEs compared to HREEs and the negative anomaly of Eu (Figure 19 c,d). In addition, in Harker diagrams, the trends of Suffi Abad rocks are similar to those of ALMC felsic rocks (Figure 6).

The intrusive rocks of Suffi Abad are I-type granites with high-K calc-alkaline affinity. Also, the magma of this intrusive series with the Sr-Nd ratios, high ratios of $^{143}Nd/^{144}Nd$ (0.5125-0.5127; Azizi et al., 2011), and low ratios of $^{87}Sr/^{86}Sr$ (0.7024-0.7069; Azizi et al., 2011)

accounts for a depleted mantle origin resulted from basalt and andesite magma in subduction regions (Azizi et al., 2011) (Figure 15). Geochemical characteristics of the intrusive rocks of Suffi Abad are almost similar to the geochemical characteristics of felsic intrusive rocks of ALMC and emplacement of these two rocks in the North of SSZ are similar.

The emplacement of intrusive rocks of ALMC in new subduction model of SSZ (Hassanzadeh and Wernicke, 2016) is presented in Figure 20a. The focus of the new subduction model of SSZ was on interpreting the discontinuous ophiolites developed in SSZ. The Zagros fold-thrust belt to the SW and the Urumieh-Dokhtar arc in the NE, are presented as the "outer" belt and "inner" belt ophiolites, respectively (e.g., Ricou,1970; Stöcklin, 1974). This claim is based on the nature of their original oceans (long-lived versus short-lived) (Figure 20 a,b) and their position (SW versus NE). The oceanic sediments in the outer belt (Zagros) ophiolites show a Triassic to Cretaceous history similar to that of the Oman ophiolite, which suggests the formation in a long-lived ocean basin (Figure 20 a,b). In contrast, sediments related to the inner belt (Khoy and Dehshir-Baft) ophiolites show the sedimentary environments in small ocean basins formed by short-lived fragmentation of the Cimmerian continental ribbon; however, igneous components in both belts are principally Late Cretaceous (99 to 93 Ma) (e.g., Davoudzadeh, 1972; Ricou, 1970; Braud, 1990) (Figure 20 a,b). In this connection, Hassanzadeh and Wernicke (2016) presented two different positions of SSZ in the new subduction model of SSZ, The position of A-A′ sections in NW of SSZ and position of B-B′ section in SE of SSZ (Figure 20 a,b). The AlMC intrusive is related to subduction area in NW of SSZ (Figure 20a).

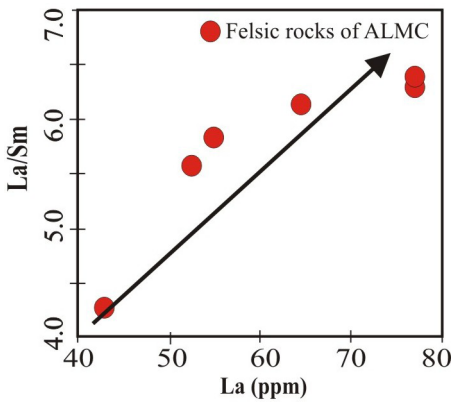

Figure 18. La/Sm vs La show increasing trend.

CONCLUSIONS

Zircon U-Pb dating demonstrates crystallization of felsic intrusive of ALMC crystallized in the Late Jurassic (148-143 Ma), similar to most of the granitic bodies in the SSZ. The isotopic date confirms that these rocks originated from the depleted mantle over the subduction zone. Moreover, the petrological microscopy, geochemical data, and zircon saturation temperature indicate that the felsic rocks of ALMC were not derived directly from the calc-alkaline andesitic or basaltic magma in the active margin. Based on the discussion in this research, the felsic rocks of ALMC have an affinity to I-type and some A-type granites that were created by melting of an I-type

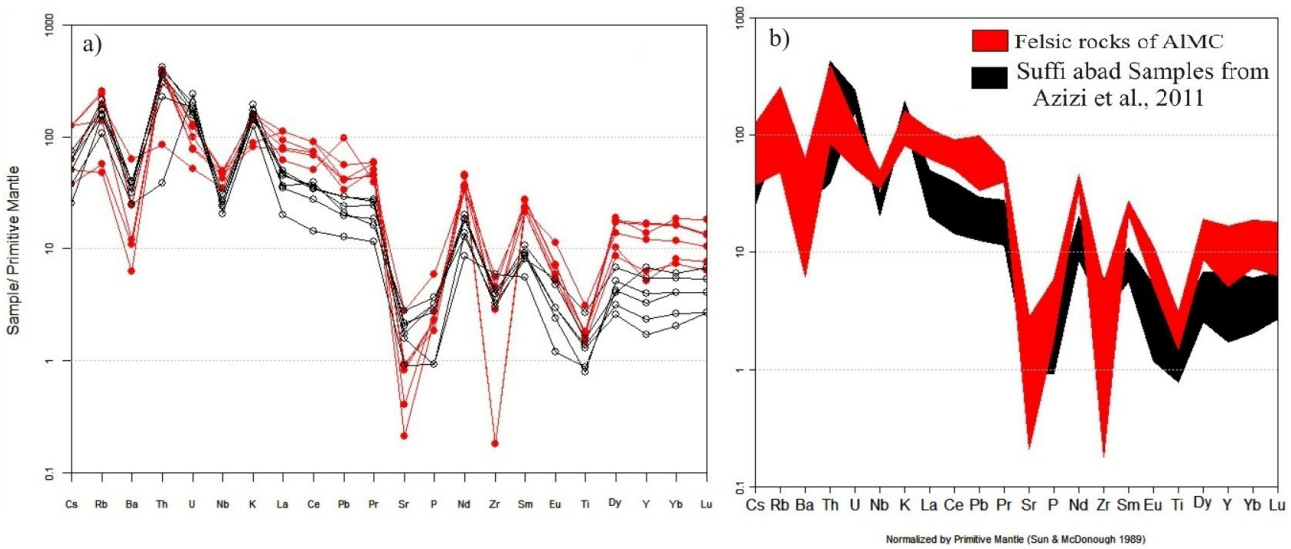

Figure 19. Normalized felsic rocks of ALMC and Suffi Abad rocks to primitive mantle (Sun and McDonough, 1989) and chondrite (Boynton, 1984). Red lines show felsic rocks of ALMC and black lines show Suffi Abad rocks after Azizi et al. (2011).

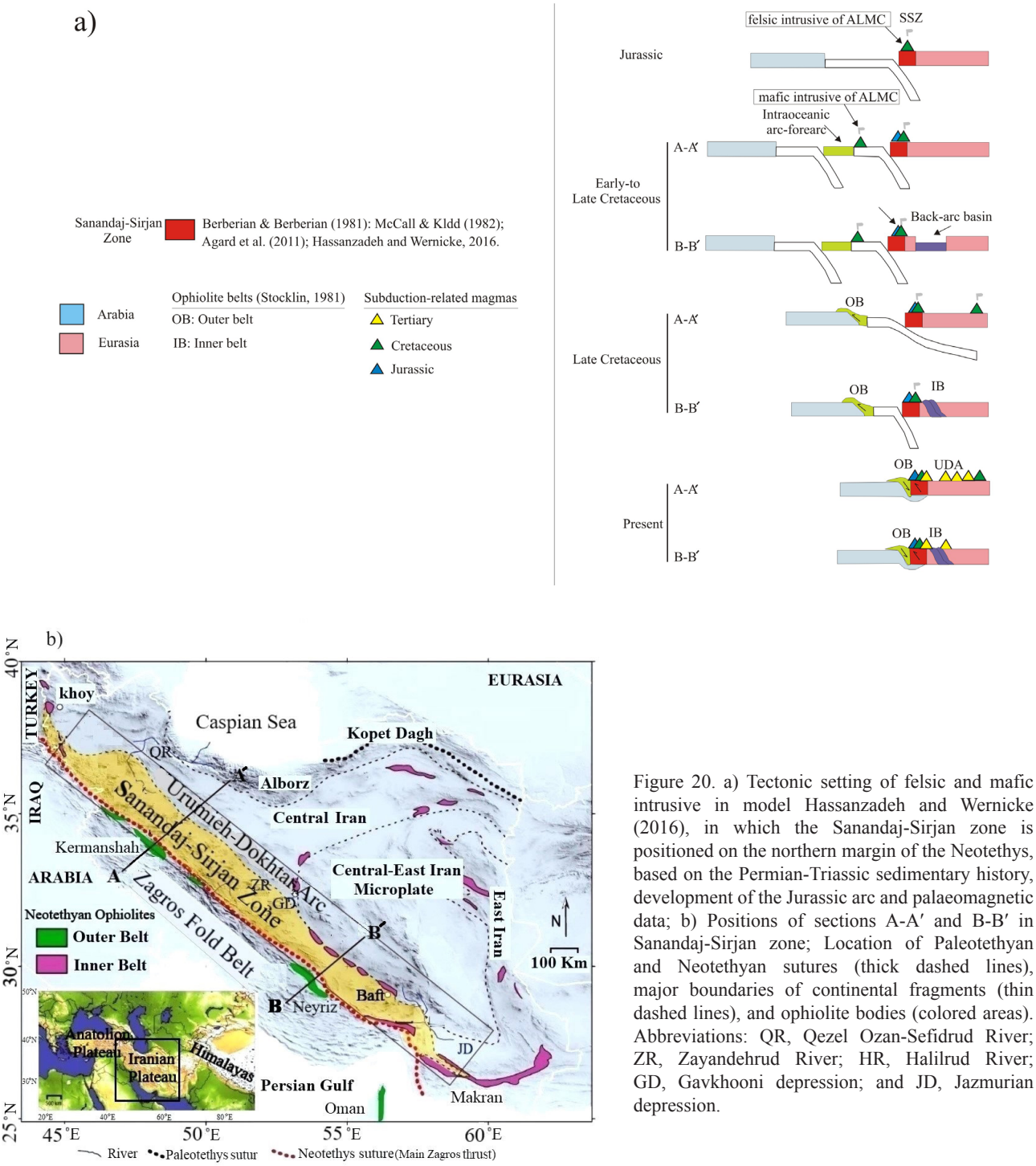

Figure 20. a) Tectonic setting of felsic and mafic intrusive in model Hassanzadeh and Wernicke (2016), in which the Sanandaj-Sirjan zone is positioned on the northern margin of the Neotethys, based on the Permian-Triassic sedimentary history, development of the Jurassic arc and palaeomagnetic data; b) Positions of sections A-A′ and B-B′ in Sanandaj-Sirjan zone; Location of Paleotethyan and Neotethyan sutures (thick dashed lines), major boundaries of continental fragments (thin dashed lines), and ophiolite bodies (colored areas). Abbreviations: QR, Qezel Ozan-Sefidrud River; ZR, Zayandehrud River; HR, Halilrud River; GD, Gavkhooni depression; and JD, Jazmurian depression.

body in the pressure lower than 4 kbar.

Mafic intrusive rocks of ALMC in subduction environment of island arc were originated in the early Cretaceous. The isotopic and geochemical data confirm that the origin of magma of this intrusive is attributed to the garnet depth stability field. In addition, the results of this research show no relationship between magma series felsic and mafic intrusive rocks of ALMC and their tectonic environment.

ACKNOWLEDGEMENTS

The authors would like to express their gratitude to assistant of Adelaide Microscopy for assistance LA-ICP-MS analysis. Field sampling and EPMA analysis was financially supported by the research grant of Payame Noor University.

REFERENCES

Agard P., Omrani J., Jolivet L., Mouthereau F., 2005. Convergence history across Zagros (Iran): constraints from collisional and earlier deformation. International Journal of Earth Sciences 94, 401-419.

Agard P., Omrani J., Jolivet L., Whitechurch H., Vrielynck B., Spakman W., Monié P., Meyer, B., Wortel R., 2011. Zagros orogeny: a subduction-dominated process. Geological Magazine 148, 692-725.

Ahadnejad V., Valizadeh M.V., Deevsalar R., Rezaei-Kahkhaei M., 2011. Age and geotectonic position of the Malayer granitoids: implication for plutonism in the Sanandaj-Sirjan Zone, W Iran. Neues Jahrbuch für Geologie und Paläontologie Abhandlungen 261, 61-75.

Ahmadi Khalaji A., Esmaeily D., Valizadeh M.V., Rahimpour-Bonab H., 2007. Petrology and geochemistry of the granitoid complex of Boroujerd, Sanandaj-Sirjan Zone, Western Iran. Journal of Asian Earth Sciences 29, 859-877.

Alavi M., 1994. Tectonics of Zagros orogenic belt of Iran: new data and interpretation. Tectonophysics 229, 211 e 238.

Allen M.B., and Armstrong H.A., 2008. Arabia-Eurasia collision and the forcing of mid-Cenozoic global cooling. Palaeogeography, Palaeoclimatology, Palaeoecology 265, 52-58.

Amiri M., Ahmad Khalaji A., Tahmasbi Z., Francisco Santos J., Zarei Sahamieh R., Zamanian H., 2017. Geochemistry, petrogenesis, and tectonic setting of the Almogholagh batholith in the SanandajeSirjan zone, western Iran. Journal of African Earth Sciences 134, 113-133.

Arvin M., Pan Y., Dargahi S., Malekizadeh A., Babaei A., 2007. Petrochemistry of the Siah-Kuh granitoid stock southwest of Kerman, Iran: implications for initiation of Neotethys subduction. Journal of Asian Earth Sciences 30, 474-489.

Ashragi S.A. and Mahmoudi Garaii M., 2003. Geological report of the Tuyserkan Sheet, scale (1:100,000). Iran Geological Survey and Mineral Exploration country, Tehran, 12 pp.

Azizi H. and Asahara Y., 2013. Juvenile granite in the Sanandaj-Sirjan zone, NW Iran: late Jurassic-early cretaceous arc-continent collision. International Geology Review 55, 1523-1540.

Azizi H. and Moinevaziri H., 2009. Review of the tectonic setting of Cretaceous to Quaternary volcanism in northwestern Iran. Journal of Geodynamics 47, 167-179.

Azizi H., Asahara Y., Mehrabi B., Chung S.L., 2011. Geochronological and geochemical constraints on the petrogenesis of high-K granite fromthe Suffi abad area, Sanandaj-Sirjan zone, NW Iran. Chemie der Erde 71, 363-376.

Azizi H., Najari M., Asahara Y., Catlos E., Shimizu M., Yamamoto K., 2015. U-Pb zircon ages and geochemistry of Kangareh and Taghiabad mafic bodies in northern Sanandaj-Sirjan Zone, Iran: Evidence for intra-oceanic arc and back-arc tectonic regime in Late Jurassic. Tectonophysics 660, 47-64.

Badr A., Davoudian A.R., Shabanian N., Azizi H., Asahara Y., Neubauer F., Dong Y., Yamamoto K., 2018. A- and I-type metagranites from the North Shahrekord Metamorphic Complex, Iran: Evidence for Early Paleozoic postcollisional magmatism. Lithos 300-301, 86-104.

Becker H., Jochum K.P., Carlson R.W., 2000. Trace element fractionation during dehydration of eclogites from high-pressure terranes and the implications for element fluxes in subduction zones. Chemical Geology 163, 65-99.

Braud J., 1990. Explanatory text of the Kermanshah quadrangle map, 1:250,000, Geological Survey of Iran, C6.

Blein O., Lapierre H., Schweickert R.A., 2001. A Permian island-arc with a continental basement: the Black Dyke Formation Nevada, North American Cordillera. Chemical Geology 175, 543-566.

Bonin B., 2007. A-type granites and related rocks: evolution of a concept problems and prospects. Lithos 97, 1-29.

Boynton W.V., 1984. Cosmochemistry of the rare earth elements: meteorite studies. In: Henderson, P. (Ed.), Rare Earth Element Geochemistry. Elsevier, Amsterdam 63-114.

Chappell B.W. and White A.J.R., 1974. Two contrasting granite types. Pacific Geology 8, 173-174.

Chappell B.W. and White A.J.R., 1992. I- and S-type granites in the Lachlan Fold Belt. Transactions of the Royal Society of Edinburgh: Earth Sciences 83, 1-26.

Chappell B.W., Bryant C.J., Wyborn D., White A.J.R., Chappell B.W., White A.J.R., Wyborn D., 1987. The importance of residual source material (restite) in granite petrogenesis. Journal of Petrology 28, 1111-1138.

Chappell B.W., Bryant C.J., Wyborn D., White A.J.R., Williams I.S., 1998. High- and low-temperature I-type granites. Resource Geology 48, 225-235.

Collins W.J., Beams S.D., White A.J.R., Chappell B.W., 1982. Nature and origin of A-type granites with particular reference to southeastern Australia: Contributions to Mineralogy and Petrology 80,189-200.

Davoudzadeh M. and Schmidt K., 1984. Contribution to the paleogeography and stratigraphy of the Upper Triassic to Middle Jurassic of Iran. Neues Jahrbuch für Geologie und Paläontologie 162, 137-163.

Eby G.N., 1990. The A-type granitoids: a review of their occurrence and chemical characteristics and speculations on their petrogenesis. Lithos 26, 115-134.

Eby G.N., Krueger H.W., Creasy J.W., 1992. Geology, geochronology, and geochemistry of the White Mountain batholith, New Hampshire, in Puffer, J.H., and Ragland, P.C., eds., Eastern North American Mesozoic magmatism: Geological Society of America Special Paper 268, 379-398.

Esna-Ashari A., Tiepolo M., Valizadeh M.V., Hassanzadeh J., Sepahi A.A., 2012. Geochemistry and zircon U-Pb geochronology of Aligoodarz granitoid complex, Sanandaj-Sirjan Zone, Iran. Journal of Asian Earth Sciences 43, 11-22.

Fazlnia A., Schenk V., Appel P., Alizade A., 2013. Petrology, geochemistry, and geochronology of the Chah-Bazargan gabbroic intrusions in the south Sanandaj-Sirjan zone, Neyriz, Iran, International Journal of Earth Sciences 102, 1403-1426.

Fazlnia A., Schenk V., Straaten F., Mirmohammadi M., 2009. Petrology, geochemistry, and geochronology of trondhjemites from the Qori Complex, Neyriz, Iran. Lithos 112, 413-433.

Ferré E.C. and Leake B.E., 2001. Geodynamic significance of early orogenic high-K crustal and mantle melts: example of the Corsica Batholithq. Lithos 59, 47-67.

Ghasemi A. and Talbot C.J., 2006. A new tectonic scenario for the Sanandaj-Sirjan Zone (Iran), Journal of Asian Earth Sciences 26, 683-693.

Hassanzadeh J. and Wernicke B.P., 2016. The Neotethyan Sanandaj-Sirjan zone of Iran as anarchetype for passive margin-arc transitions. Tectonics 35, 586-621.

Hassanzadeh J., Stockli D.F., Horton B.K., Axen G.J., Stockli L.D., Grove M., Schmitt A.K., Walker J.D., 2008. U-Pb zircon geochronology of late Neoproterozoic-Early Cambrian granitoids in Iran: implications for paleogeography, magmatism, and exhumation history of Iranian basement. Tectonophysics 451, 71-96.

Hunziker D., Burg J.P., Bouilhol P., von Quadt A., 2015. Jurassic rifting at the Eurasian Tethys margin: Geochemical and geochronological constraints from granitoids of North Makran, southeastern Iran, Tectonics 34, 571-593.

Jackson S.E., Pearson N.J., Griffin W.L., Belousova E.A., 2004. The application of laser ablation-inductively coupled plasma-mass spectrometry to in situ U-Pb zircon geochronology. Chemical Geology 211, 47-69.

Jahn B.M., Fuyuan W., Chen B., 2000. Massive granitoid generation in Central Asia: Nd isotope evidence and implication for continental growth in the Phanerozoic. Episode 23, 82-92.

Jamshidi Badr M., Collins A., Masoudi F., Cox G., Mohajjel M., 2013. The U-Pb age, geochemistry and tectonic significance of granitoids in the Soursat Complex, Northwest Iran. Turkish Journal of Earth Sciences 22, 1-31.

Jamshidi Badr M., Masoudi F., Collins A.S., Cox G., 2010. Dating of Precambrian metasedimentary rocks and timing of their metamorphism in the Soursat metamorphic complex (NW IRAN): Using LA-ICP-MS, U-Pb Dating of Zircon and Monazite, Journal of Sciences, Islamic Republic of Iran 21, 311-319.

Jamshidi badr M., Masoudi F., Collins A.S., Sorbi A., 2012. Mineralogical Evidence for Regional Metamorphism Overprinted By Contact Metamorphism. Acta Geologica Sinica 86, 48-64.

Jamshidibadr M., 2013. The Impact of Different Orogenic Phases on Deformation and Metamorphic of Volcano Sedimentary Rocks in the Almabulage Complex (NW of Iran). Geodynamics Research International Bulletin 1, 25-37 (in Persian).

Jiang Y.H., Jia R.Y., Liu Z., Liao S.Y., Zhao P., Zhou Q., 2013. Origin of Middle Triassic high-K calc-alkaline granitoids and their potassic microgranular enclaves from the western Kunlun orogen, northwest China: a record of the closure of Paleo-Tethys, Lithos 156-159, 13-30.

Keay S.M., Collins W.J., Mcculloch M.T., 1997. A three-component mixing model for granitoid genesis: Lachlan Fold Belt, eastern Australia. Geology 25, 307-310.

King P.L., Chappell B.W., Allen C.M., White A.J.R., 2001. Are A-type granites the high temperature felsic granites? Evidence from fractionated granites of the Wangrah Suite. Australian Journal of Earth Sciences 48, 501-514.

Le Maitre R.W. (Ed.), Bateman P., Dubek A., Keller J., Lameyre J., Le Bas M.J., Sabine P.A., Schmid R., Sırensen H., Streckeisen A., Woolley A.R., Zanettin B., 1989. A Classification of Igneous Rocks and Glossary of Terms. Recommendations of the International Union of Geological Sciences Subcommission on the Systematics of Igneous Rocks, Blackwell, Oxford, 193 pp.

Loiselle M.C. and Wones D.R., 1979. Characteristics and origin of anorogenic granites. Geological Society of America Abstract with Program 11, 468.

Mahmoudi S., Corfu F., Masoudi F., Mehrabi B., Mohajjel M., 2011. U-Pb dating and emplacement history of granitoid plutons in the northern Sanandaj-Sirjan Zone, Iran. Journal of Asian Earth Sciences 41, 238-249.

Maniar P.D. and Piccoli P.M., 1989. Tectonic discrimination of granitoids. Geological Society of American Bulletin 101, 635-643.

Middlemost E.A.K., 1994. Naming materials in the magma/igneous rock system. Earth Science Review 37, 215-224.

Mohajjel M., Fergusson C.L., Sahandi M.R., 2003. Cretaceous-Tertiary convergence and continental collision, Sanandaj-Sirjan Zone, western Iran. Journal of Asian Earth Sciences 21, 397-412.

Moritz R., Ghazban F., Singer B.S., 2006. Eocene gold ore formation at Muteh, Sanandaj-Sirjan tectonic zone, Western Iran: A result of late-stage extension and exhumation of metamorphic basement rocks within the Zagros Orogen. Economic Geology 101, 1497-1524.

Mouthereau F., 2011. Timing of uplift in the Zagros belt/Iranian plateau and accommodation of late Cenozoic Arabia/Eurasia convergence. Geological Magazine 148, 726-738.

Muttoni G., Kent D.V., Garzanti E., Brack P., Abrahamsen N., Gaetani M., 2003. Early permian pangea 'B'to late permian pangea 'A'. Earth and Planetary Science Letters 215, 379-394.

Okay A.I. and Tüysüz O., 1999. Tethyan sutures of northern Turkey. Geological Society, London, Special Publications 156, 475-515.

Okay A.I., Zattin M., Cavazza W., 2010. Apatite fission-track data for the Miocene Arabia-Eurasia collision. Geology 38, 35-38.

Patiño Douce A.A. and Beard J.S., 1995. Dehydration-melting of biotite gneiss and quartz amphibolite from 3 to 15 kbar. Journal of Petrology 36, 707-738.

Patiño Douce A.E., 1997. Generation of metaluminous A-type granites by lowpressure melting of calc-alkaline granitoids. Geology 25, 743-746.

Patiño Douce A.E., 1999. What do experiments tell us about relative contributions of crust and mantle to the origin of granitic magma? In: Castro A., Fernandez C., Vigneress J.L. (Eds.), Understanding Granites: Integrating New and Classification Techniques. Geological Society, London, Special Publications 168, 55-75.

Payne J.L., Barovich K., Hand M., 2006. Provenance of metasedimentary rocks in the northern Gawler Craton, Australia: implications for Palaeoproterozoic reconstructions. Precambrian Research 148, 275-291.

Pearce J.A., Harris B.W., Tindle A.G., 1984. Trace element discrimination diagrams for the tectonic interpretation of granitic rocks: Journal of Petroleum 25, 956-983.

Peccerillo A. and Taylor S.R., 1976. Geochemistry of Eocene calc-alkaline volcanic rocks from the Kastamonu area, northern Turkey: Contributions to Mineralogy and Petrology 58, 63-81.

Peters B.J. and Day J.M.D., 2014. Assessment of relative Ti, Ta, and Nb (TITAN) enrichments in ocean island basalts, Geochemistry, Geophysics, Geosystems 15, 4424-4444.

Plank T. and Langmuir C.H., 1998. The chemical composition of subducting sediment and its consequences for the crust and mantle. Chemical Geology 145, 325-394.

Rickwood P.C., 1989. Boundary lines within petrologic diagrams which use oxides of major and minor elements. Lithos 22, 247-264.

Ricou E., 1970. Comments on radiolarite and ophiolite nappes in the Iranian, Geological Magazine 479-480.

Ricou L.E., 1994. Tethys Reconstructed-Plates, Continental Fragments and Their Boundaries since 260-Ma from Central-America to South-Eastern Asia. Geodinamica Acta 7, 169-218.

Roberts M.P. and Clemens J.D., 1993. Origin of high potassium, calc-alkaline I-type granitoids. Geology 21, 825-828.

Rolland Y., Billo S., Corsini M., Sosson M., Galoyan G., 2009. Blueschists of the Amassia-Stepanavan Suture Zone (Armenia): linking Tethys subduction history from E-Turkey to W-Iran, International Journal of Earth Sciences 98, 533-550.

Rollinson H.R., 1993. Using geochemical data: Evaluation, presentation, interpretation. Harlow, Essex, England: Longman Scientific & Technical, 352 pp.

Sarjoughian F., Kananian A., Haschke M., Ahmadian J., 2015. Transition from I-type to A-type magmatism in the Sanandaj-Sirjan Zone, NW Iran: An extensional intra-continental arc, Geology Journal 51, 387-404.

Shahbazi H., Siebel W., Ghorbani M., Pourmoafee M., Sepahi A.A., Vousoughi Abedini M., Shang C.K., 2015. The Almogholagh pluton, Sanandaj-Sirjan zone, Iran: geochemistry, U-(Th)-Pb titanite geochronology and implications for its tectonic evolution., Neues Jahrbuch für Mineralogie-Abhandlungen. Journal of Mineralogy and Geochemistry 192, 85-99.

Shahbazi H., Siebel W., Pourmoafee M., Ghorbani M., Sepahi A.A., Shang C.K., Vosoughi Abedini M., 2010. Geochemistry and U-Pb zircon geochronology of the Alvand plutonic complex in Sanandaj-Sirjan Zone (Iran): new evidence for Jurassic magmatism. Journal of Asian Earth Sciences 9, 668-683.

Sheikholeslami M.R., Pique A., Mobayen P., Sabzehei M., Bellon H., Hashem Emami M., 2008. Tectono-metamorphic evolution of the Neyriz metamorphic complex, Quri- Kor-e-Sefid area (Sanandaj-Sirjan Zone, SW Iran). Journal of Asian Earth Sciences 31, 504-521.

Sisson T.W., Ratajeski K., Hankins W.B., Glazner A.F., 2005. Voluminous granitic magmas from common basaltic sources. Contributions to Mineralogy and Petrology 148, 635-661.

Skjerlie K.P. and Johnston A.D., 1993. Vapor-absent melting at 10 kbar of a biotite and amphibole bearing tonalitic gneiss, implications for the generation of A-type granites. Geology 20, 263-266.

Soesoo A., 2000. Fractional crystallization of mantle-derived melts as a mechanism for some I-type granite petrogenesis: an example from Lachlan Fold Belt, Australia. Journal of the Geological Society 157, 135-149.

Stampfli G.M. and Borel G.D., 2002. A plate tectonic model for the Paleozoic and Mesozoic constrained by dynamic plate boundaries and restored synthetic oceanic isochrons. Earth and Planetary Science Letters 196, 17-33.

Sun S.S. and McDonough W.F., 1989. Chemical and isotopic systematic of oceanic basalts: Implication for mantle composition and processes, in Sunders AD, Norry MJ (Eds.), Magmatic in oceanic basins. Special Publication. Geology Society of London 42, 313-345.

Sylvester P.J., 1989. Post-collisional alkaline granites. Journal of Geology 97, 261-280.

Tian S.H., Yang Z.S., Hou Z.Q., Mo X.X., Hu W.J., Zhao Y., Zhao X.Y., 2015. Subduction of the Indian lower crust beneath southern Tibet revealed by the postcollisional potassic and ultrapotassic rocks in SW Tibet. Gondwana Research 41, 29-50.

Trifonov V., Ivanova T., Bachmanov D., 2012. Evolution of the central Alpine-Himalayan belt in the Late Cenozoic. Russian Geology and Geophysics 53, 221-233.

Valizadeh M.V. and Zarian S., 1976. A petrological study of the Almogholagh, Asadabad and Hamedan plutons. Journal of Sciences, Islamic Republic of Iran 8, 49-59 (in Persian with

English abstract).
Van Achterbergh E., Ryan C.G., Jackson S.E., Griffin W.L., 2001. Data reduction software for LA-ICP-MS. In: Sylvester Paul J. (Ed.), Laser-Ablation-ICPMS in the Earth Sciences: Principles and Applications. Mineralogical Association of Canada 239-243.
Wang G.C., Jiang Y.H., Liu Z., Ni C.Y., Qing L., Zhang Q., 2015. Elemental and Sr-Nd-Hf isotopic constraints on the origin of Late Jurassic adakitic granodiorite in central Fujian province, southeast China. Mineralogy and Petrology 109, 501-518.
Watson E.B. and Harrison T.M., 1983. Zircon saturation revisited: temperature and composition effects in a variety of crustal magma types. Earth and Planetary Science Letters 64, 295-304.
Whalen J.B., Currie K.L., Chappell B.W., 1987. A-type granites: geochemical characteristics, discrimination and petrogenesis. Contributions to Mineralogy and Petrology 95, 407-419.
Whitney D.L. and Evans B.W., 2010. Abbreviations for names of rock-forming minerals, American Mineralogist 95, 185-187.
Yajam S., Monterro P., Scarrow J.H., Ghalamghash J., Razavi S.M.H., Bea F., 2015. The spatial and compositional evolution of the Late Jurassic Ghorveh-Dehgolan plutons of the Zagros Orogen, Iran: SHRIMP zircon U-Pb and Sr and Nd isotope evidence. Geologica Acta 13, 25-43.